beings. *Lancet* **362**: 371–373.

29. Tsarev, S. A., Emerson, S. U., Tsareva, T. S., Yarbough, P. O., Lewis, M., Govindarajan, S., Reyes, G. R., Shapiro, M. and Purcell, R. H. 1993. Variation in course of hepatitis E in experimentally infected cynomolgus monkeys. *J. Infect. Dis.* **167**: 1302–1306.
30. Watanabe, T., Katagiri, J., Kojima, H., Kamimura, T., Ichida, F., Ashida, M., Hamada, C. and Shibayama, T. 1987. Studies on transmission of human non-A, non-B hepatitis to marmosets. *J. Med. Virol.* **22**: 143–156.

JOURNAL OF VIROLOGY, Oct. 2007, p. 10890–10896 Vol. 81, No. 20
0022-538X/07/$08.00+0 doi:10.1128/JVI.00807-07

Latent Infection of a New Alphanodavirus in an Insect Cell Line[▽]

Tian-Cheng Li,[1]* Paul D. Scotti,[2] Tatsuo Miyamura,[1] and Naokazu Takeda[1]

Department of Virology II, National Institute of Infectious Diseases, Gakuen 4-7-1, Musashi-Murayama, Tokyo 208-0011, Japan,[1] and Waiatarua, Auckland, New Zealand[2]

Received 14 April 2007/Accepted 26 July 2007

Insect BTI-TN-5B1-4 (Tn5) cells have been used extensively with recombinant baculoviruses to express foreign genes. When a recombinant baculovirus containing the hepatitis E virus capsid protein gene was used to infect Tn5 cells, unknown virus particles in addition to the anticipated hepatitis E virus-like particles were produced in the infected cells. The unknown virus particles were 35 nm in diameter and contained RNA that was highly homologous to full-length RNA1 (3,107 bp) and RNA2 (1,383 bp) genomic RNAs of flock house virus. Surprisingly, both RNAs seen in these induced nodavirus particles could be amplified from commercially available Tn5 cells without infection with or induction by a baculovirus. The nucleotide sequences from the purified nodavirus particles and the normal Tn5 cells were identical, demonstrating that the Tn5 cells themselves were latently infected with a nodavirus. However, the generation of nodavirus particles was significantly stimulated by infection with recombinant baculoviruses. Phylogenetic analysis suggested that this new nodavirus belongs to the genus *Alphanodavirus* in the family *Nodaviridae*.

The family *Nodaviridae* comprises small, nonenveloped, and isometric viruses containing positive-sense bipartite RNA genomes (3, 26). Two genera in this family, *Alphanodavirus* and *Betanodavirus*, have been distinguished previously (2). Alphanodaviruses infect primarily insects, but their general pathogenicity is not well defined. However, the type virus, Nodamura virus, causes paralysis in infected larvae of the wax moth, *Galleria mellonella* (1), suckling mice (23, 24), and suckling hamsters (8). In addition to Nodamura virus, the genus *Alphanodavirus* includes flock house virus (FHV), black beetle virus, Boolarra virus, and Pariacoto virus (5, 22, 23, 28, 32). Viruses belonging to the genus *Betanodavirus* infect primarily fishes and are the causative agent of viral encephalopathy and retinopathy and viral nervous necrosis, a devastating disease of many species of marine fish cultured worldwide (19). Although a number of betanodavirus strains have been isolated from fish, only five alphanodaviruses have been isolated. Recently, an unclassified nodavirus, *Macrobrachium rosenbergii* nodavirus, was isolated from the giant freshwater prawn, *M. rosenbergii* (29).

Nodavirus particles are 32 to 33 nm in diameter, and their buoyant density in CsCl ranges from 1.30 to 1.34 g/cm^3 (25). The virion has icosahedral symmetry with T=3 and is composed of 180 copies of a single coat protein of around 40 kDa (12, 30). The genome is composed of two RNA segments, RNA1 (3.1 kb) and RNA2 (1.4 kb). RNA1 carries all the viral information required for RNA transcription and replication and encodes protein A (102 kDa) and protein B (10 kDa). Protein A is a catalytic subunit of the RNA-dependent RNA polymerase that functions in the replication of both RNA segments. RNA2 encodes the coat precursor protein alpha, which is cleaved into beta (38-kDa) and gamma (5-kDa) proteins during the maturation of the particle, a reaction essential for infectivity (27). Both RNA1 and RNA2 are required for infection and are packaged in the same virion (21). Both RNAs have 5′-cap structures, while their 3′ ends lack poly(A) tails (5, 10, 14, 20). During RNA replication, the RNA-dependent RNA polymerase directs the production of the subgenomic RNA3, which encodes nonstructural proteins B1 and B2 in overlapping open reading frames. Nodaviruses provide outstanding model systems for the study of RNA replication, virus assembly, and three-dimensional structure (3, 26).

In our laboratory, the recombinant baculovirus expression system has been a major tool for the generation of recombinant virus proteins. Two insect cell lines, Sf9 and Tn5, were routinely used. During the purification of hepatitis E virus-like particles (HEV-LP) from recombinant baculovirus-infected Tn5 cells, we found a large amount of a 40-kDa protein (p40). This protein appeared to form virus particles similar to those of nodaviruses. Antigenic analysis showed that p40 was cross-reactive with anti-FHV antibody. Further studies detected that full-length RNA1 and RNA2 genomes were present in normal insect cells, suggesting that these Tn5 cells were latently infected with a nodavirus.

MATERIALS AND METHODS

Insect cells. The insect BTI-TN-5B1-4 cell line ("High Five"), which we have designated Tn5/97, was derived from BTI-TN-5B1-4 (Tn5) and was obtained in April 1997 from a commercial supplier (Invitrogen Inc.; lot BAC0010CB). This cell line has been regularly employed for the expression of various viral capsid proteins by using recombinant baculoviruses (11, 15, 17). EX-CELL 400 or EX-CELL 405 medium (JRH Biosciences, Lenexa, KS) was used to maintain Tn5/97 cells. A different lot of the same cell line, designated Tn5/05, was obtained on 6 October 2005 from the same commercial supplier (Invitrogen Inc.; lot 1288466). Another insect cell line, Sf9, was obtained from Riken BioResource Center, Tsukuba-shi, Japan, and maintained in TC-100 medium (GIBCO BRL, Gaithersburg, MD). *Drosophila melanogaster* Schneider 2 (S2) cells, an insect cell line derived from *D. melanogaster* embryos, were obtained from Invitrogen Inc. and grown at 28°C in Schneider's insect medium supplemented with 10% heat-inactivated fetal bovine serum, 10 U of penicillin per ml, and 10 μg of streptomycin per ml. S2 cells were routinely passaged every 4 days at a 1:5 dilution.

Recombinant baculoviruses. Wild-type baculovirus (*Autographa californica* nuclear polyhedrosis virus) and the following recombinant baculoviruses were used in this study: Ac[G3n13ORF2] (unpublished data), Ac[G3ORF2] (unpublished data),

* Corresponding author. Mailing address: Department of Virology II, National Institute of Infectious Diseases, Gakuen 4-7-1, Musashi-Murayama, Tokyo 208-0011, Japan. Phone: (81) 42-561-0771. Fax: (81) 42-561-4729. E-mail: litc@nih.go.jp.

▽ Published ahead of print on 8 August 2007.

Ac[G1ORF2] (17), Ac[G4ORF2] (unpublished data), Ac[G1HEV] (unpublished data), Ac[G4ORF3] (unpublished data), Ac[NoroVP1] (11), Ac[BKVP1] (15), Ac[JCVP1] (unpublished data), Ac[TTVORF2] (unpublished data), Ac[polioVP1] (unpublished data), and Ac[NodaRNA2] (1,000 × *g*) harboring, respectively, the hepatitis E virus (HEV) genotype 3 *ORF2* gene with a deletion corresponding to the N-terminal 13 amino acids of the product, full-length HEV genotype 3 *ORF2*, HEV genotype 1 *ORF2*, HEV genotype 4 *ORF2*, the full-length genome of HEV genotype 1, HEV genotype 4 *ORF3*, the norovirus genogroup I genotype 2 VP1 gene, the human BK polyomavirus VP1 gene, the human polyomavirus JC VP1 gene, transfusion-transmitted virus *ORF2*, the poliovirus VP1 gene, and the nodavirus RNA2, which was derived from the Tn5/97 cell line. The generation of the recombinant baculoviruses and the preparation of the seed virus were performed using Sf9 cells; protein expression was carried out with Tn5 cells.

Amplification of nodavirus RNA by reverse transcription-PCR (RT-PCR). Total RNA from cell lysates, culture media, or purified virus particles was extracted with RNAzol-LS reagent (Invitrogen Inc., Carlsbad, CA). The extracted RNA was resuspended in 20 μl of DNase-, RNase-, and proteinase-free distilled water. Reverse transcription was performed at 42°C for 50 min and at 70°C for 15 min in a 20-μl reaction mixture containing 1 μl of Superscript II RNase H reverse transcriptase (Invitrogen Inc.), 1 μl of the primer, 1 μl of RNaseOUT, 2 μl of 0.1 M dithiothreitol, 4 μl of 5× RT buffer, 1 μl of 10 mM deoxynucleoside triphosphates, 5 μl of RNA, and 5 μl of distilled water. The reverse primer Noda-U7 (5′-ACCTCTGCCCTTTCGGGCTA-3′; nucleotides [nt] 3088 to 3107) was used for the cDNA synthesis of RNA1, and Noda-U1 (5′-ACCTTAGTCTGTTGACTTAA-3′; nt 1381 to 1400) was used for RNA2. Primers were designed on the basis of FHV (GenBank accession no. X15959).

The entire RNA1 was obtained as two overlapping fragments. The 5′-end half of the genome was amplified with the forward primer Noda-D6 (5′-GTTTTCG AAACAAATAAAACAGAAAA-3′; nt 1 to 26) and the reverse primer Noda-U9 (5′-CTTCAGGTTCAGCATCAGGA-3′; nt 2061 to 2080). The 3′-end half of the genome was amplified with the forward primer Noda-D7 (5′-AGCA CTGGACTGCGAAACCA-3′; nt 421 to 440) and the reverse primer Noda-U7. The entire RNA2 was obtained similarly with a set of primers for the 5′-end half of the genome, Noda-D1 (5′-GTAAACAATTCCAAGTTCCA-3′; nt 1 to 20) and Noda-U2 (5′-GAGGATTTAATGATGGATTT-3′; nt 1133 to 1152), and a set of primers for the 3′ end of the genome, Noda-D2 (5′-CAACGAGCTCAA CGCGTTGT-3′; nt 50 to 69) and Noda-U1.

PCR was performed in a 50-μl reaction mixture containing 2 μl of cDNA, 0.25 μl of ExTaq DNA polymerase (Takara Shuzo Co., Ltd., Kyoto, Japan), 1 μl of the forward primer, and 1 μl of a reverse primer. Each cycle consisted of denaturation at 95°C for 30 s, primer annealing at 55°C for 30 s, and an extension reaction at 72°C for 180 s, and the last cycle was followed by a final extension at 72°C for 7 min. The PCR products were purified using a QIAquick PCR purification kit (QIAGEN, Hilden, Germany) and cloned into the TA cloning vector pCR2.1 (Invitrogen, Carlsbad, CA).

To amplify part of the RNA2 molecule, PCR was carried out using the forward primer Noda-D4 (5′-ACATCCAGATCCGATCAAGT-3′; nt 491 to 510) and the reverse primer Noda-U4 (5′-GCCAGGAATGTTGCTTGCAA-3′; nt 1161 to 1180). Each cycle consisted of denaturation at 95°C for 30 s, primer annealing at 55°C for 30 s, and an extension reaction step at 72°C for 45 s; the procedure was completed by a final extension step at 72°C for 7 min.

The nucleotide sequencing of PCR products and plasmids was carried out with the primers used for the amplification by using an ABI 3130 genetic analyzer automated sequencer and a BigDye Terminator cycle sequencing ready reaction kit according to the instructions of the manufacturer (Applied Biosystems, Foster City, CA).

Purification of nodavirus particles from recombinant baculovirus-infected Tn5 cells. The recombinant baculovirus-infected Tn5/97 cells were harvested at 7 days postinfection (p.i.). The medium and the cells were separated by centrifugation at 1,000 × *g* for 15 min at 4°C. The cells were treated with a denaturation buffer containing 50 mM sodium borate, 150 mM NaCl, 1% Nonidet P-40, 0.5% sodium deoxycholate, and 5% 2-mercaptoethanol and gently rocked at room temperature for 2 h. The lysate was diluted with EX-CELL 405 and centrifuged at 31,000 rpm for 3 h in a Beckman SW32 Ti rotor, and the pellet was resuspended in EX-CELL 405. For sucrose gradient centrifugation, 100-μl samples were laid on the top of a 10 to 50% (wt/wt) gradient and centrifuged at 32,000 rpm for 2 h in a Beckman SW55 Ti rotor. For CsCl gradient centrifugation, 4.5-ml samples were mixed with 2.1 g of CsCl and centrifuged at 35,000 rpm for 24 h at 10°C in the same rotor. The gradient was fractionated into 250-μl aliquots, and each fraction was weighed in order to estimate the buoyant density and isopycnic point. Each fraction was diluted with EX-CELL 405 and centrifuged for 2 h at 50,000 rpm in a Beckman TLA55 rotor to sediment the virus particles.

Electron microscopy. Samples containing the nodavirus particles were applied onto apioloform-coated grids, and the particles were allowed to attach to the grids for 5 min. After a rinse with distilled water, each sample was stained with 1% aqueous uranyl acetate and observed by using a Hitachi H-7000 electron microscope at 75 kV.

N-terminal amino acid sequence analysis. The proteins separated by sodium dodecyl sulfate-polyacrylamide gel electrophoresis (SDS-PAGE) were visualized by staining with GelCode blue staining reagent (Pierce, Rockford, IL) and purified by using TALON resin (BD Biosciences Clontech, Palo Alto, CA). The N-terminal amino acid microsequencing was carried out using 100 pmol of the protein for Edman automated degradation on an Applied Biosystems model 477 protein sequencer.

SDS-PAGE and Western blot assay. The proteins in the cell lysate and culture medium were separated by 5 to 20% SDS-PAGE and stained with Coomassie blue. For Western blot assays, the proteins in the SDS-polyacrylamide gel were electrophoretically transferred onto a nitrocellulose membrane. The membrane was then blocked with 5% skim milk in a solution of 50 mM Tris-HCl (pH 7.4) and 150 mM NaCl and incubated with the serum from a hepatitis E patient that was positive for anti-HEV immunoglobulin G (IgG) and IgM or with rabbit anti-FHV IgG antibody. Alkaline phosphatase-conjugated goat anti-human Ig (1:3,000 dilution; Dako A/S, Copenhagen, Denmark) or alkaline phosphatase-conjugated goat anti-rabbit Ig (1:1,000 dilution; Chemicon, Temecula, CA) was used as the secondary antibody. Nitroblue tetrazolium chloride and BCIP (5-bromo-4-chloro-3-indolylphosphate) *p*-toluidine were used as coloring agents (Bio-Rad Laboratories, Hercules, CA).

Infectivity of purified nodavirus particles. Subconfluent *Drosophila* S2 cells (5 × 10^5 cells) in a 25-cm^2 flask were infected with 1 ml (100 ng) of purified nodavirus particles. The virus was allowed to attach for 2 h at 28°C. The medium containing any unattached virus particles was removed, and 10 ml of fresh medium was added. Infected S2 cells were passaged every 4 days at a 1:5 dilution. Cells and supernatants were collected and assayed for nodavirus coat protein by the Western blot method using rabbit anti-FHV coat protein antibody.

Nucleotide sequence accession numbers. The nodavirus RNA sequences determined in this study have been deposited in GenBank under accession numbers EF690537 (RNA1) and EF690538 (RNA2).

RESULTS

Induction of nodavirus virion formation by recombinant baculovirus infection. A recombinant baculovirus, Ac[G3n13ORF2], harboring the HEV genotype 3 *ORF2* with the region corresponding to the N-terminal 13 amino acids of the product deleted, was used to generate HEV-LP in Tn5/97 cells. When the HEV-LP were purified by CsCl centrifugation and each fraction was analyzed by SDS-PAGE, three major proteins with molecular masses of 40 kDa (p40), 53 kDa (p53), and 64 kDa (p64) were observed (Fig. 1A). Proteins p64 and p53 appeared in fractions 9 and 10 and fractions 12 and 13, which had average densities of 1.300 g/ml^3 and 1.285 g/ml^3, respectively. Both p64 and p53 were reactive with the serum from a patient with acute hepatitis E, indicating that these two proteins were derived from the HEV protein (Fig. 1B). However, another protein, p40, was detected in fractions 5, 6, and 7, which had an average density of 1.350 g/ml^3. A Western blot assay indicated that p40 did not react with the serum from the hepatitis E patient (Fig. 1B).

The N-terminal amino acid sequence of p40 was determined by microsequencing, and the sequence VNNSRPKRQRS QRVV was obtained. This sequence is close to the 15-amino-acid N-terminal sequence (VNNNRPRRGRAQRVV) of FHV, a nodavirus in the genus *Alphanodavirus*. Surprisingly, when a Western blot assay was performed with rabbit anti-FHV coat protein, p40 showed strong reactivity. A minor protein with a molecular mass of 43 kDa (p43) also appeared in fraction 6. Although p43 did not react with the serum from the hepatitis E patient, like p40, it reacted with the anti-FHV

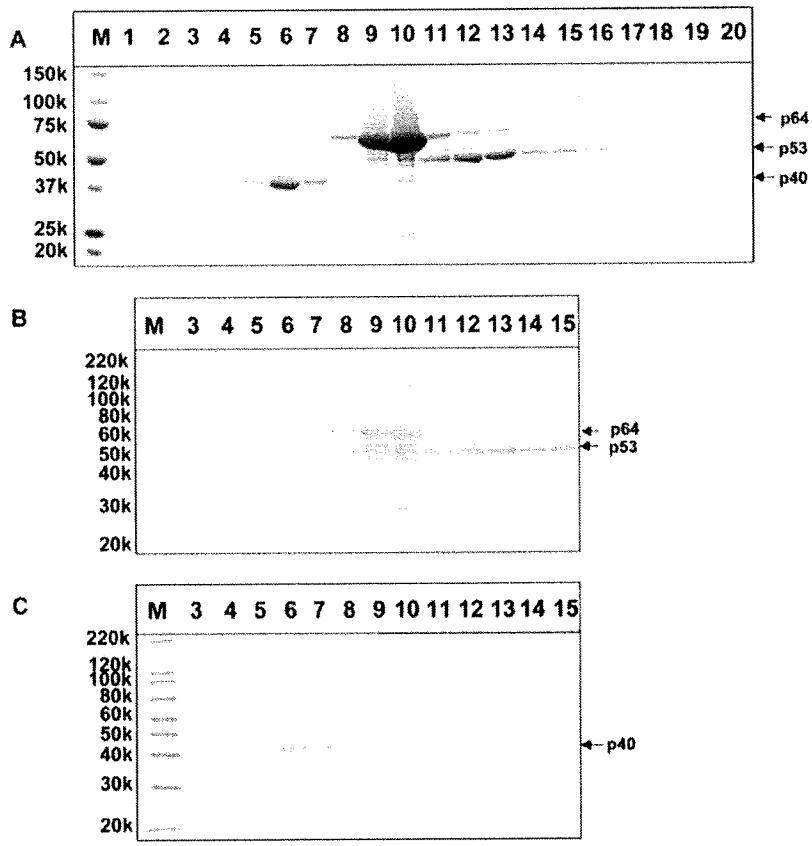

FIG. 1. Induction of p40 protein by a recombinant baculovirus infection. (A) The HEV-LP recovered from Ac[G3n13ORF2]-infected Tn5/97 cells were purified by CsCl gradient centrifugation. The gradient was fractionated into 250-μl aliquots, and the proteins were separated by 5 to 20% SDS-PAGE and stained with Coomassie blue. (B and C) Each fraction was subjected to a Western blot assay using either the serum from a patient with acute hepatitis E (B) or rabbit anti-FHV coat protein antibody (C). M, molecular weight markers; 150k, molecular weight of 150,000.

antibody (Fig. 1C). In addition, the N-terminal amino acid sequence of p43 was identical to that of p40 (data not shown). When fraction 6 was examined by electron microscopy, many small spherical particles with diameters of 35 nm were observed. These particles were similar to FHV particles (Fig. 2). These results indicated that p43 and p40 were derived from the 35-nm-diameter particles and that infecting the Tn5/97 cells with the recombinant baculovirus Ac[G3n13ORF2] induced not only the expression of the HEV ORF2 proteins but also the formation of nodavirus-like particles.

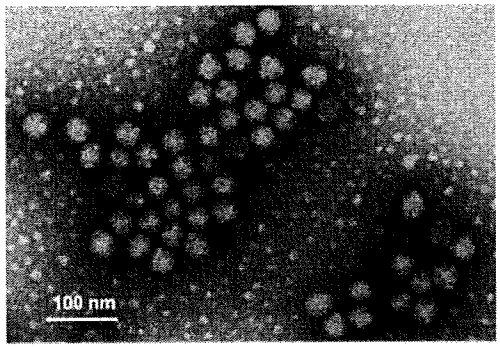

FIG. 2. Electron micrograph of nodavirus-like 35-nm particles. Fraction 6 from Fig. 1 was used for electron microscopy observations.

Amplification of nodavirus RNA2 genome from Tn5 cells. To determine which cell and/or virus stock was contaminated with the nodavirus, total RNA was extracted from lysates and culture media from uninfected Tn5/97 cells, uninfected Sf9 cells, Ac[G3n13ORF2]-infected Tn5/97 cells, and Ac[G3n13ORF2]-infected Sf9 cells. Part of the RNA2 sequence (nt 491 to 1180) was then amplified by RT-PCR. As shown in Fig. 3, a band corresponding to 690 bp from both the lysates and culture media from uninfected Tn5/97 cells and Ac[G3n13ORF2]-infected Tn5/97 cells was detected (Fig. 3, lanes 1, 2, 5, and 6) whereas no band from either uninfected or Ac[G3n13ORF2]-infected Sf9 cells was detected (Fig. 3, lanes 3, 4, 7, and 8). These results indicated that neither the Sf9 cells nor the seed baculovirus had been contaminated with RNA2. To confirm that the nodavirus sequence was derived from the Tn5 cells, a new lot of Tn5 cells (Tn5/05) was purchased. A 200-μl aliquot of the cell suspension was removed from the original tube, the cells were separated from the culture medium, and RT-PCR was performed to determine if a region of the RNA2 sequence was present. Both the cells and the medium were positive for the 690-bp band, clearly indicating that the Tn5/05 cells had been infected, presumably latently, with a nodavirus (Fig. 3, lanes 9 and 10).

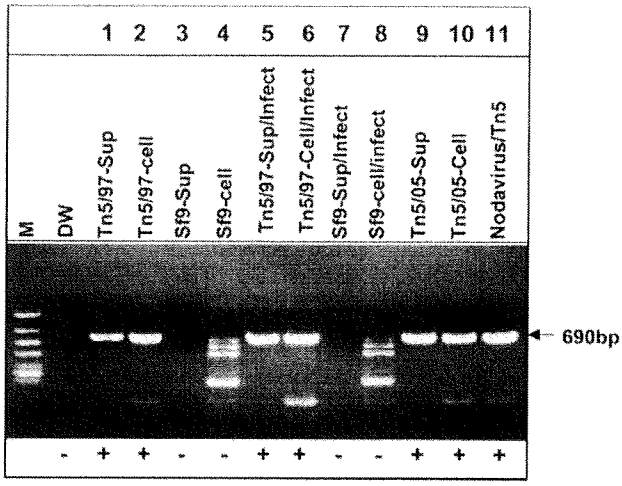

FIG. 3. Amplification of part of the nodavirus RNA2 from insect cells and from purified nodavirus-like particles. RNA was extracted from the supernatant and lysate from uninfected Tn5/97 cells (Tn5/97-sup and Tn5/97-cell), uninfected Sf9 cells (Sf9-sup and Sf9-cell), Ac[G3n13ORF2]-infected Tn5/97 cells (Tn5/97-sup/infect and Tn5/97-cell/infect), Ac[G3n13ORF2]-infected Sf9 cells (Sf9-sup/infect and Sf9-cell/infect), and uninfected Tn5/05 cells (Tn5/05-sup and Tn5/05-cell). RNA was also extracted from nodavirus-like particles purified from an Ac[G3n13ORF2]-infected Tn5/97 cell lysate (nodavirus/Tn5). A 690-bp segment corresponding to a region of RNA2 was amplified with the primers RNA2-D4 and RNA2-U2. M, molecular weight markers; DW, distilled water.

Amplification of full-length RNA1 and RNA2 genomic RNAs from nodavirus like-particles and uninfected Tn5 cells. The nodavirus like-particles purified from Ac[G3n13ORF2]-infected Tn5/97 cells had a density in CsCl similar to those of nodaviruses. Electron microscopy indicated that these particles contained nucleic acid(s) (Fig. 2). To determine if the particles contained RNA homologous to the nodavirus genome, RNA was extracted from purified particles and amplified by RT-PCR. Two fragments, one of 3,107 bp and the other of 1,383 bp, similar in length to FHV RNA1 and RNA2, were obtained. The nucleotide identity between the 3,107-bp fragment and FHV RNA1 was 89.3%; that between the 1,383-bp fragment and FHV RNA2 was 77.6%. No comparable amplification was observed when RNA extracted from purified HEV-LP was used (data not shown). These results indicated that the nodavirus like-particles purified from Ac[G3n13ORF2]-infected Tn5/97 cells contained a complete nodavirus genome.

To further characterize this putative nodavirus, full-length RNA1 and RNA2 were amplified from both the lysate and the culture medium obtained from uninfected Tn5/97 cells. The nucleotide sequences of these RNAs were 100% identical to those of the RNAs extracted from the particles purified from Ac[G3n13ORF2]-infected Tn5/97 cells. These results again indicated that uninfected Tn5 cells were latently infected with a nodavirus. Phylogenetic analysis based on the amino acid sequence of the coat protein precursor, encoded in the 1,383-bp fragment corresponding to RNA2, indicated that this virus belongs to the genus *Alphanodavirus* in the family *Nodaviridae* (Fig. 4). We have designated this virus Tn5 cell line (TNCL) virus.

Induction of TNCL virus coat protein expression by recombinant baculoviruses. To characterize the induction of the expression of the p40 and p43 proteins, Ac[G3n13ORF2]-infected Tn5/97 cells were harvested daily for 10 days p.i. The proteins generated in infected cells were separated by SDS-PAGE and analyzed by a Western blot assay using the rabbit anti-FHV coat protein antibody (Fig. 5). Although the TNCL virus-specific protein was not detected before 2 days p.i., p43 appeared in the cells at 3 days p.i. At 5 days p.i., two bands corresponding to p40 and p43 were observed. These proteins were not apparent in uninfected Tn5/97 cells (Fig. 5, lane C), whereas a faint band corresponding to p43 was observed in wild-type baculovirus-infected cells (Fig. 5, lane W). The p43 was thought to be the coat protein precursor, and p40 was the mature coat protein. To confirm that p43 and p40 were derived from RNA2, a recombinant baculovirus, Ac[NodaRNA2], comprising the entire TNCL virus RNA2 genome was generated and used to infect Sf9 cells. In Ac[NodaRNA2]-infected Sf9 cells, both p43 and p40 were detected by a Western blot assay after 5 days p.i. (Fig. 6).

In addition to Ac[G3n13ORF2] and Ac[NodaRNA2], we examined other recombinant baculoviruses, including Ac[G1ORF2], Ac[G3ORF2], Ac[G4ORF2], Ac[G1HEV], Ac[G4ORF3], Ac[NoroVP1], Ac[BKVP1], Ac[JCVP1], Ac[TTVORF2], and Ac[polioVP1]. The recombinant baculovirus-infected Tn5/97 cells were harvested at 5 days p.i., and the various cell lysates were analyzed by Western blot assays (Fig. 6). The nodavirus coat protein was detected in the wild type-infected and all the recombinant baculovirus-infected cell lysates but not in uninfected Tn5 and Sf9 cell lysates (Fig. 6, lanes Tn5-cell and Sf9-cell). We also infected Sf9 cells with the above-named recombinant baculoviruses, but no coat protein was detected (data not shown). These results indicated that the expression of TNCL virus coat protein was induced only when Tn5 cells were infected with either the wild-type or a recombinant baculovirus.

TNCL virus is infectious in *Drosophila* S2 cells. To determine whether TNCL virus particles purified from Tn5 cells were infectious, *Drosophila* S2 cells were infected with purified TNCL virus particles and harvested at each of eight passages. The presence of TNCL virus coat protein was assayed by Western blotting. As shown in Fig. 7, coat protein was detected at passages 1 through 8 but was not detected in uninfected S2 cells. The amount of coat protein decreased from passage 1 through passage 4 but then increased from passage 5 through passage 8. Coat protein was not detected in the supernatants (data not shown). If TNCL virus was not infectious, then the amount of the coat protein in the cells should have decreased steadily with repeated passaging because of the 1:5 dilution at each passage. The coat protein observed in passage 1 through 4 was presumably derived from the remaining TNCL virus used for the infection. However, the amount of the coat protein obviously increased from passage 5 through passage 8, clearly indicating that TNCL virus was capable of infecting S2 cells. These results indicated that at least some TNCL virus particles were infectious.

DISCUSSION

A latent infection of a widely used *Trichoplusia ni*-derived insect cell line, Tn5, by a previously undescribed nodavirus,

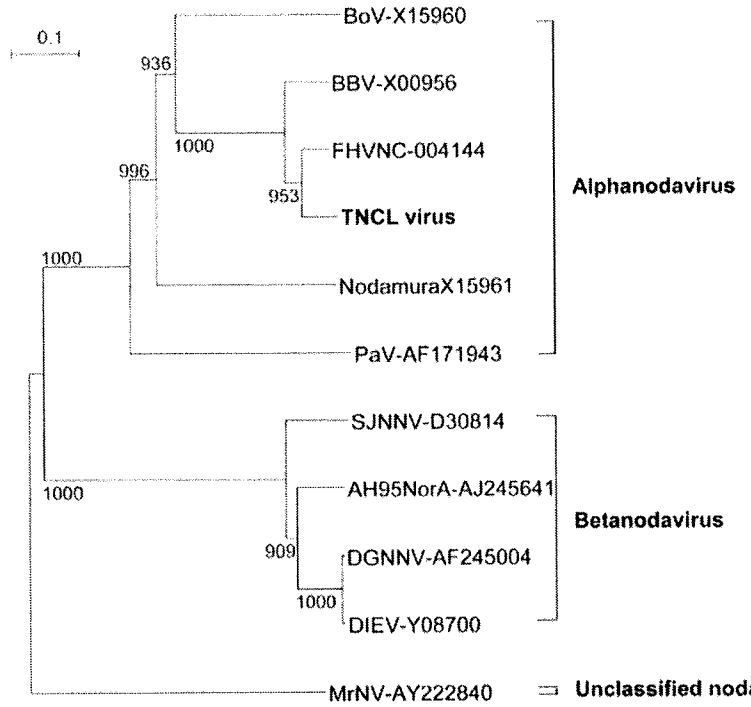

FIG. 4. Phylogenetic analysis of TNCL virus on the basis of the coat protein precursor. The deduced amino acid sequence of the coat protein precursor was analyzed by the neighbor-joining method. Representative nodavirus strains and the corresponding accession numbers are indicated. The coat protein precursor from *M. rosenbergii* nodavirus (MrNV; accession no. AY222840) was used as an out-group. The bootstrap values correspond to 1,000 replications. BoV, Boolarra virus; BBV, black beetle virus; Nodamura, Nodamura virus; PaV, Pariacoto virus; SJNNV, striped jack nervous necrosis virus; AH95NorA, Atlantic halibut virus; DGNNV, dragon grouper nervous necrosis virus; DIEV, *Dicentrarchus labrax* encephalitis virus.

TNCL virus, was accidentally disclosed following the infection of the cells with a recombinant baculovirus. A similar infection of a *D. melanogaster* cell line by a nodavirus had been reported previously (7), so such unapparent infections with nodaviruses may not be uncommon. Since these infections may present no obvious symptoms in the cell cultures, detection may occur only serendipitously. Such infections may go undetected for years.

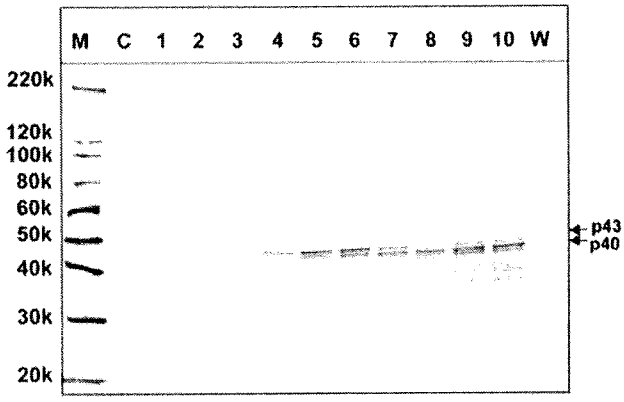

FIG. 5. TNCL virus coat protein synthesis in Ac[G3n13ORF2]-infected Tn5 cells. Tn5/97 cells grown in a 25-cm^2 flask were infected with Ac[G3n13ORF2] at a multiplicity of infection of 10 and incubated at 26.5°C. On days 1 through 10 p.i. (lanes 1 through 10, respectively), the cell lysates were separated by 5 to 20% SDS-PAGE and analyzed by a Western blot assay with rabbit anti-FHV antibody. M, molecular weight markers; C, uninfected Tn5/97 cells (control); W, wild-type baculovirus-infected Tn5/97 cells; 220k, molecular weight of 220,000.

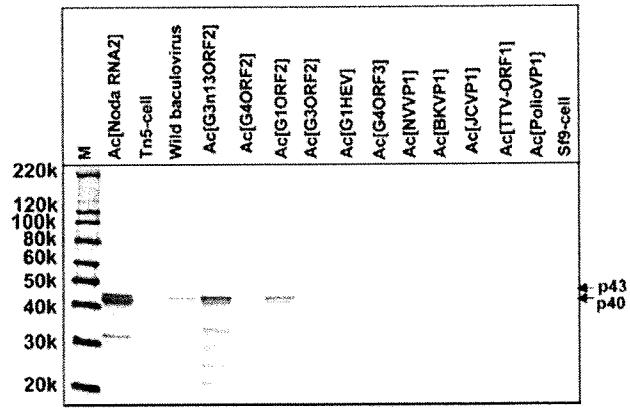

FIG. 6. Induction of TNCL virus coat protein synthesis by various recombinant baculoviruses. Tn5/97 cells were infected with the indicated 11 recombinant baculoviruses and wild-type (wild) baculovirus. The cells were harvested at 5 days p.i., and the cell lysates were analyzed by Western blot assays using rabbit anti-FHV coat protein antibody. M, molecular weight markers; Ac[NodaRNA2], cell lysate from Ac[NodaRNA2]-infected Sf9 cells; Tn5-cell, uninfected Tn5/97 cells; Sf9-cell, uninfected Sf9 cells; 220k, molecular weight of 220,000.

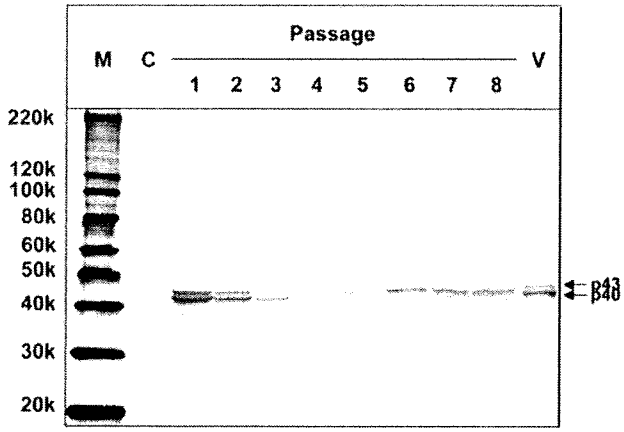

FIG. 7. Infectivity of TNCL virus particles purified from Tn5 cells. *Drosophila* S2 cells were infected with purified TNCL virus particles and passaged every 4 days at a 1:5 dilution. The lysates from uninfected S2 cells (control [C]) and infected S2 cells (passages 1 through 8) were separated by 5 to 20% SDS-PAGE. The coat protein of TNCL virus was detected by a Western blot assay with rabbit anti-FHV coat protein antibody. M, molecular weight markers; V, purified TNCL virus particles; 220k, molecular weight of 220,000.

Phylogenetic analysis of the virus described here (TNCL virus) indicates that it belongs to the genus *Alphanodavirus*. Wild-type baculovirus itself was capable of inducing the TNCL virus, so the foreign virus genes contained within the recombinant baculovirus genomes were not in themselves responsible for the induction. However, the inducing ability seems to be dependent on the inserted foreign genes as well as the expressed protein(s) (Fig. 6). As TNCL virus coat protein was detected only when wild-type or recombinant baculovirus was used to infect the Tn5 cells and other stresses like heat shock and cold shock did not induce the expression of the virus coat protein (data not shown), the translation and replication of the nodavirus genome seemed to be activated by the baculovirus infection. However, the mechanism by which baculovirus infection activates TNCL virus replication is unclear at moment. Mutant baculoviruses may provide a clue to the mechanism. At this time, we do not know the gene(s) or the mechanism for the stimulated expression of p40 and p43 and the particle formation.

Full-length genomic RNA1 and RNA2 of TNCL virus were detected in the two lots of uninfected Tn5 cells, one obtained in 1997 (Tn5/97) and subcultured since then and the second obtained in 2005 (Tn5/05), suggesting that these commercially available Tn5 cells had been infected latently with this virus. The nucleotide sequence of TNCL virus was closest to that of FHV among the alphanodaviruses (Fig. 4), and Western blot assays demonstrated that the coat protein was cross-reactive with anti-FHV antibody, suggesting that TNCL virus was antigenically similar to FHV. Nodamura virus, black beetle virus, FHV, and Boolarra virus have been shown to be cross-reactive with one another by double-diffusion immunoprecipitation tests; however, they represent different serotypes (25). Whether TNCL virus is serologically different from other alphanodaviruses is not clear. The nucleotide sequence homologies between the genomes of TNCL virus and FHV were 89.3% for RNA1 and 77.6% for RNA2. The amino acid homologies between proteins A and the coat protein precursors alpha were 83.36% and 89.68%, respectively. In addition, when the nucleotide sequences of TNCL virus and FHV were compared, we found that the RNA2 of TNCL virus lacked 17 bases present at the end of the RNA2 of FHV corresponding to the C terminus (nt 1248 to 1264). These results suggest that the TNCL virus is a new species of the genus *Alphanodavirus*.

The recombinant baculovirus expression system is routinely used for the production of foreign proteins. Two insect cell lines, derived from *Spodoptera frugiperda* (Sf9) and *Trichoplusia ni* (Tn5 [BTI-Tn-5B1-4]), are frequently used (9, 31). Tn5 cells have better secretion, which results in a higher productivity of recombinant proteins with the baculovirus expression system. Initial reports demonstrated that Tn5 cells produce at least 20-fold more secreted alkaline phosphatase than the Sf9 or Sf2l cell lines (6). The recombinant baculovirus expression system has also been employed for the efficient production of virus-like particles from different sources. Because virus-like particles closely mimic the properties of native virions, virus-like particles are attractive molecular candidates for recombinant vaccines. In fact, virus-like particles derived from HEV, hepatitis C virus, human BK polyomavirus, human polyomavirus JC, and human papillomavirus have been prepared using this expression system (4, 13, 16, 18).

Commercially available Tn5 cells were found to be latently infected with TNCL virus, and the infectious virus was induced by recombinant baculovirus infection. Unfortunately, this means that there is a serious risk of contamination by TNCL virus when virus-like particles are produced using this system. Although no alphanodavirus infections of humans have been reported, the type virus, Nodamura virus, is unique in being capable of infecting suckling mice and suckling hamsters (8, 23, 24), with resulting paralysis and death. When virus-like particles are considered for use as a vaccine, it is essential that the nodavirus, present as the result of a latent, unapparent infection, be removed. All cell lines derived from the insect Tn5 cell line should be examined for the presence of such nodaviruses. Because of the ability of nodaviruses to establish latent and unapparent infections, all insect cell lines should be screened routinely for the presence of virus.

ACKNOWLEDGMENTS

We thank Tomoko Mizoguchi and Satoko Ogawa for secretarial work.

The study was supported in part by grants including Research on Emerging and Re-emerging Infectious Diseases, Research on Hepatitis, and Research on Food Safety from the Ministry of Health, Labor and Welfare, Japan.

REFERENCES

1. **Bailey, L., and H. A. Scott.** 1973. The pathogenicity of Nodamura virus for insects. Nature **241**:545.
2. **Ball, L. A., D. A. Hendry, J. E. Johnson, R. R. Rueckert, and P. D. Scotti.** 2000. Nodavirus RNA replication: mechanism and harnessing to vaccinia virus recombinants. Academic Press, San Diego, CA.
3. **Ball, L. A., and K. L. Johnson.** 1998. Nodaviruses of insects. Plenum, New York, NY.
4. **Baumert, T. F., J. Vergalla, J. Satoi, M. Thomson, M. Lechmann, D. Herion, H. B. Greenberg, S. Ito, and T. J. Liang.** 1999. Hepatitis C virus-like particles synthesized in insect cells as a potential vaccine candidate. Gastroenterology **117**:1397–1407.
5. **Dasmahapatra, B., R. Dasgupta, A. Ghosh, and P. Kaesberg.** 1985. Structure of the black beetle virus genome and its functional implications. J. Mol. Biol. **182**:183–189.

6. **Davis, T. R., T. J. Wickham, K. A. McKenna, R. R. Granados, M. L. Shuler, and H. A. Wood.** 1993. Comparative recombinant protein production of eight insect cell lines. In Vitro Cell Dev. Biol. Anim. **29A**:388–390.
7. **Friesen, P., P. Scotti, J. Longworth, and R. Rueckert.** 1980. Black beetle virus: propagation in Drosophila line 1 cells and an infection-resistant subline carrying endogenous black beetle virus-related particles. J. Virol. **35**: 741–747.
8. **Garzon, S., H. Strykowski, and G. Charpentier.** 1990. Implication of mitochondria in the replication of Nodamura virus in larvae of the Lepidoptera, Galleria mellonella (L.) and in suckling mice. Arch. Virol. **113**:165–176.
9. **Granados, R. R., C. G. D. Anja, and G. D. Kathleen.** 1986. Replication of the Trichoplusia ni granulosis and nuclear polyhedrosis viruses in cell cultures. Virology **152**:472–476.
10. **Guarino, L. A., A. Ghosh, B. Dasmahapatra, R. Dasgupta, and P. Kaesberg.** 1984. Sequence of the black beetle virus subgenomic RNA and its location in the viral genome. Virology **139**:199–203.
11. **Hansman, G. S., K. Natori, H. Shirato-Horikoshi, S. Ogawa, T. Oka, K. Katayama, T. Tanaka, T. Miyoshi, K. Sakae, S. Kobayashi, M. Shinohara, K. Uchida, N. Sakurai, K. Shinozaki, M. Okada, Y. Seto, K. Kamata, N. Nagata, K. Tanaka, T. Miyamura, and N. Takeda.** 2006. Genetic and antigenic diversity among noroviruses. J. Gen. Virol. **87**:909–919.
12. **Hosur, M. V., T. Schmidt, R. C. Tucker, J. E. Johnson, T. M. Gallagher, B. H. Selling, and R. R. Rueckert.** 1987. Structure of an insect virus at 3.0 A resolution. Proteins **2**:167–176.
13. **Ishii, Y., S. Ozaki, K. Tanaka, and T. Kanda.** 2005. Human papillomavirus 16 minor capsid protein L2 helps capsomeres assemble independently of intercapsomeric disulfide bonding. Virus Genes **31**:321–328.
14. **Kaesberg, P., R. Dasgupta, J. Y. Sgro, J. P. Wery, B. H. Selling, M. V. Hosur, and J. E. Johnson.** 1990. Structural homology among four nodaviruses as deduced by sequencing and X-ray crystallography. J. Mol. Biol. **214**:423–435.
15. **Li, T. C., N. Takeda, K. Kato, J. Nilsson, L. Xing, L. Haag, R. H. Cheng, and T. Miyamura.** 2003. Characterization of self-assembled virus-like particles of human polyomavirus BK generated by recombinant baculoviruses. Virology **311**:115–124.
16. **Li, T. C., N. Takeda, T. Miyamura, Y. Matsuura, J. C. Wang, H. Engvall, L. Hammar, L. Xing, and R. H. Cheng.** 2005. Essential elements of the capsid protein for self-assembly into empty virus-like particles of hepatitis E virus. J. Virol. **79**:12999–13006.
17. **Li, T. C., Y. Yamakawa, K. Suzuki, M. Tatsumi, M. A. Razak, T. Uchida, N. Takeda, and T. Miyamura.** 1997. Expression and self-assembly of empty virus-like particles of hepatitis E virus. J. Virol. **71**:7207–7213.
18. **Matsuo, E., H. Tani, C. Lim, Y. Komoda, T. Okamoto, H. Miyamoto, K. Moriishi, S. Yagi, A. H. Patel, T. Miyamura, and Y. Matsuura.** 2006. Characterization of HCV-like particles produced in a human hepatoma cell line by a recombinant baculovirus. Biochem. Biophys. Res. Commun. **340**:200–208.
19. **Munday, B. L., J. Kwang, and N. Moody.** 2002. Betanodavirus infections of teleost fish. J. Fish Dis. **25**:127–142.
20. **Newman, J. F., and F. Brown.** 1976. Absence of poly (A) from the infective RNA of Nodamura virus. J. Gen. Virol. **30**:137–140.
21. **Newman, J. F., and F. Brown.** 1978. Further physicochemical characterization of Nodamura virus. Evidence that the divided genome occurs in a single component. J. Gen. Virol. **38**:83–95.
22. **Reinganum, C., J. B. Bashiruddin, and G. F. Cross.** 1985. Boolarra virus: a member of the Nodaviridae isolated from Oncopera intricoides (Lepidoptera: Hepialidae). Intervirology **24**:10–17.
23. **Scherer, W. F., and H. S. Hurlbut.** 1967. Nodamura virus from Japan: a new and unusual arbovirus resistant to diethyl ether and chloroform. Am. J. Epidemiol. **86**:271–285.
24. **Scherer, W. F., J. E. Verna, and W. Richter.** 1968. Nodamura virus, an ether- and chloroform-resistant arbovirus from Japan: physical and biological properties, with ecologic observations. Am. J. Trop. Med. Hyg. **17**:120–128.
25. **Schneemann, A., L. A. Ball, C. Delsert, J. E. Johnson, and T. Nishizawa (ed.).** 2004. Virus taxonomy. Eighth report of the International Committee on Taxonomy of Viruses. Elsevier/Academic Press, London, United Kingdom.
26. **Schneemann, A., V. Reddy, and J. E. Johnson.** 1998. The structure and function of nodavirus particles: a paradigm for understanding chemical biology. Adv. Virus Res. **50**:381–446.
27. **Schneemann, A., W. Zhong, T. M. Gallagher, and R. R. Rueckert.** 1992. Maturation cleavage required for infectivity of a nodavirus. J. Virol. **66**:6728–6734.
28. **Scotti, P. D., S. Dearing, and D. W. Mossop.** 1983. Flock House virus: a nodavirus isolated from Costelytra zealandica (White) (Coleoptera: Scarabaeidae). Arch. Virol. **75**:181–189.
29. **Sri Widada, J., S. Durand, I. Cambournac, D. Qian, Z. Shi, E. Dejonghe, V. Richard, and J. R. Bonami.** 2003. Genome-based detection methods of Macrobrachium rosenbergii nodavirus, a pathogen of the giant freshwater prawn, Macrobrachium rosenbergii dot-blot, in situ hybridization and RT-PCR. J. Fish Dis. **26**:583–590.
30. **Wery, J. P., V. S. Reddy, M. V. Hosur, and J. E. Johnson.** 1994. The refined three-dimensional structure of an insect virus at 2.8 A resolution. J. Mol. Biol. **235**:565–586.
31. **Wickham, T. J., and G. R. Nemerow.** 1993. Optimization of growth methods and recombinant protein production in BTI-Tn-5B1-4 insect cells using the baculovirus expression system. Biotechnol. Prog. **9**:25–30.
32. **Zeddam, J. L., J. L. Rodriguez, M. Ravallec, and A. Lagnaoui.** 1999. A noda-like virus isolated from the sweetpotato pest *Spodoptera eridania* (Cramer) (Lep.; Noctuidae). J. Invertebr. Pathol. **74**:267–274.

Arch Virol (2008) 153:2291–2295
DOI 10.1007/s00705-008-0248-x

BRIEF REPORT

Efficient production of type 2 porcine circovirus-like particles by a recombinant baculovirus

Lan-Jun Liu · Takako Suzuki · Hiroshi Tsunemitsu · Michiyo Kataoka · Noriyo Ngata · Naokazu Takeda · Takaji Wakita · Tatsuo Miyamura · Tian-Cheng Li

Received: 29 June 2008 / Accepted: 16 October 2008 / Published online: 9 November 2008

Abstract The capsid protein of PCV2 was expressed by using a recombinant baculovirus with insect Tn5 cells. A large amount of 28-kDa protein was released into the culture medium and self-assembled into PCV2-like particles (PCV2-LPs) with a buoyant density of 1.365 g/cm^3 and a diameter of 20 nm. PCV2-LPs were efficiently expressed, yielding 1 mg of purified particles per 10^7 Tn5 cells. The PCV2-LPs have antigenicity similar to that of authentic PCV2 particles, allowing us to develop a method for sensitively detecting PCV2-specific IgG antibodies. In addition, the PCV2-LPs appeared to be the most promising PCV2 vaccine candidate, by virtue of their potent immunogenicity.

Postweaning multisystemic wasting syndrome (PMWS) is a disease with low morbidity but high mortality in swine. PMWS has a serious economic impact on the global swine industry. It was first reported in western Canada in 1991 and later identified in the United States, Mexico, Europe, and Asia [2]. Porcine circovirus type 2 (PCV2) is the primary causative agent of PMWS, though the etiology of this disease has not been fully elucidated. The isolation of viruses from tissues of affected swine led to the identification of PCV2 [5–8, 20]. PCV2, a member of the family *Circoviridae* [25], is a small spherical nonenveloped virus with a single-stranded closed circular genomic DNA of 1.7 kb in length [1]. Two major open reading frames (ORFs) oriented in opposite directions have been identified. ORF1 encodes two proteins: Rep and its truncated form, Rep′, both of which are essential for viral DNA replication. ORF2 encodes a major structural protein that has type-specific epitopes [17, 22] and is very immunogenic and strongly associated with the induction of neutralizing antibodies [24], suggesting its potential use in diagnostic assays as well as vaccine development. In the present study, we expressed the PCV2 capsid protein by using a recombinant baculovirus in Tn5 insect cells. The capsid protein self-assembled into PCV2-like particles (PCV2-LPs) and was released into the culture medium. The PCV2-LPs possess similar antigenicity to that of the native PCV2 particles and appear to be a good antigen for the sensitive detection of PCV2-specific antibodies. Our study also demonstrated that PCV2-LPs are the most promising PCV2 vaccine candidate.

Viral DNA was extracted from the PCV2 Yamagata strain [23], and the full-length ORF2 of PCV2 (PCV2-ORF2) was amplified by PCR with forward primer PCV2-D1 (5′-AA**GGATCC**ATGACGTATCCAAGGAGGCGTT-3′) and reverse primer PCV2-U1 (5′-GC**TCTAGA**TTAGGGT TTAAGTGGGGGGTCT-3′). The forward primer contained the *Bam*HI site before the start codon, and the reverse primer

L.-J. Liu · N. Takeda · T. Wakita · T. Miyamura · T.-C. Li (✉)
Department of Virology II, National Institute of Infectious Diseases, Gakuen 4-7-1, Musashi-murayama, Tokyo 208-0011, Japan
e-mail: litc@nih.go.jp

T. Suzuki · H. Tsunemitsu
Research Team for Viral Diseases, National Institute of Animal Health, Kannondai 3-1-5, Tsukuba, Ibaraki 305-0856, Japan

L.-J. Liu
Chengdu Institute of Biological Products, No. 379, 3rd Section, Jinhua Road, Jinjiang District, 610023 Chengdu, Sichuan, China

M. Kataoka · N. Ngata
Department of Pathology, National Institute of Infectious Diseases, Gakuen 4-7-1, Musashi-murayama, Tokyo 208-0011, Japan

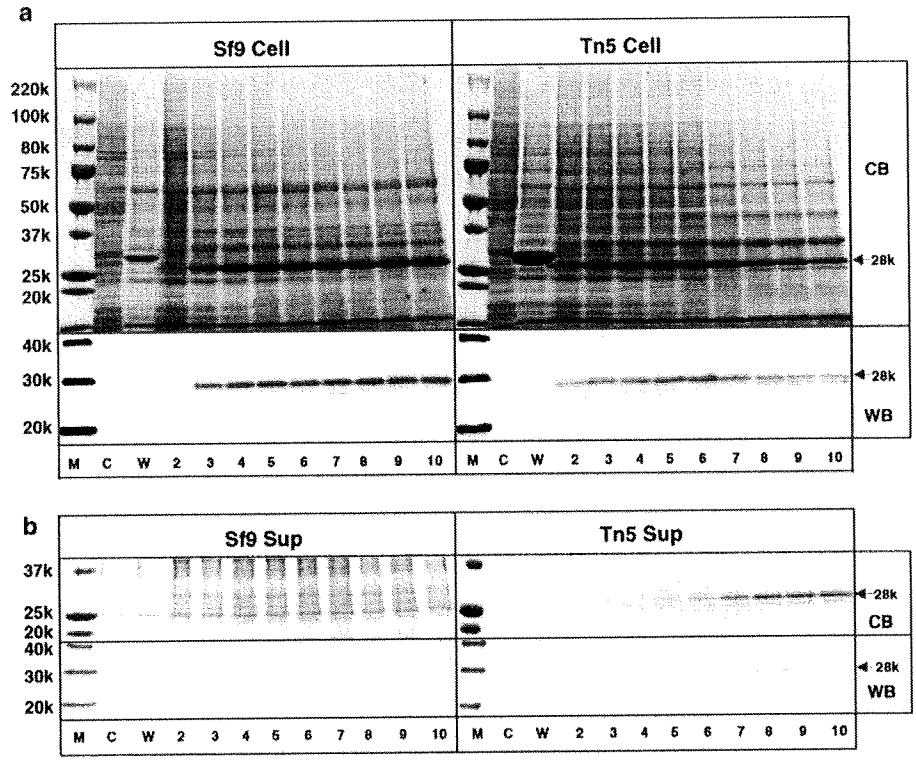

Fig. 1 Time course of the expression of PCV2 capsid protein in insect cells. Insect Sf9 and Tn5 cells were infected with the recombinant baculovirus AcPCV2-ORF2, incubated at 26.5°C, and harvested on the indicated days (2–10 days). Five microliters of the culture medium and the lysate from 10^6 cells were analyzed by SDS-PAGE. Protein bands were visualized by Coomassie blue staining (*CB*) or by Western blot assay with anti-PCV2 rabbit serum (*WB*). The cell lysate (**a**) and culture medium (**b**) were analyzed separately. *M* molecular weight marker, *C* uninfected cell, *W* wild-type baculovirus-infected cells, *lanes* 2–10, 2–10 days p.i

contained the *Xba*I site after the stop codon. The amplified ORF2 fragment was purified by using a gel extraction kit (Qiagen, Valencia, CA) and was first digested with *Bam*HI and then partially digested with *Xba*I. The purified 700-bp fragment was ligated into transfer vector pVL1393 (Pharmingen, San Diego, CA) by a ligation kit (Takara, Shiga, Japan), and a transfer plasmid pVL1393/PCV2-ORF2 was constructed.

A recombinant baculovirus was constructed and capsid proteins were expressed as previously described [14, 16]. Insect Sf9 and Tn5 cells were infected with a recombinant baculovirus, AcPCV2-ORF2, containing the entire PCV2 capsid protein. The infected cells were harvested daily until 10 days p.i. The proteins expressed in infected cells were analyzed by SDS-PAGE followed by Coomassie blue staining and by Western blot assay using a rabbit anti-PCV2 antibody (Fig. 1). A major band with a molecular mass of 28 kDa was observed in cell lysate of both Sf9 and Tn5 cells (Fig. 1a). The 28-kDa protein was first detected on day 2 in both Sf9 and Tn5 cells, and peaked on day 5 p.i. This 28-kDa protein was detected on day 4 p.i. in the supernatant of Tn5 cells and increased until day 10 p.i. (Fig. 1b), whereas it was not detected in the supernatant of Sf9 cells.

The culture medium of the AcPCV2-ORF2-infected Tn5 cells was harvested at 7 days p.i., and the PCV2 capsid protein was purified by CsCl gradient centrifugation. The 28-kDa protein appeared mainly in fractions 3, 4, and 5, which had an average density of 1.365 g/ml[3] (Fig. 2a). Examination of these fractions by electron microscopy revealed spherical particles with diameters of ~20 nm. The morphology of these particles was similar to that of the authentic PCV2 particles (Fig. 2b), indicating that the 28-kDa protein formed virus-like particles (VLPs) (PCV2-LPs). The yield of the purified VLPs was 1 mg per 10^7 Tn5 cells in culture medium. We tried to purify the PCV2 capsid protein from the infected Sf9 cells, but only a few PCV2-LPs were obtained from the cell lysate, and no VLPs were obtained from the supernatant (data not shown).

An ELISA to detect antibodies was developed by using PCV2-LPs as an antigen. This antibody ELISA showed a low background, probably because the PCV2-LPs were highly purified. The cutoff value of IgG was determined by using 30 serum samples from wild boar that were negative for anti-PCV2 IgG by Western blot assay (data not shown). The OD values of these sera were between 0.036 and 0.249, and the mean value was 0.062 with a standard deviation (SD) of 0.046. Therefore, the cutoff value, the mean value+3SD, was calculated as 0.200. The PCV2-specific IgG elicited in swine experimentally infected with the PCV2 Yamagata strain was detected by the antibody ELISA. As depicted in Fig. 3a, significant IgG antibody titers were observed, indicating that the purified PCV2-LPs had similar antigenicity to native PCV2. A panel of 105

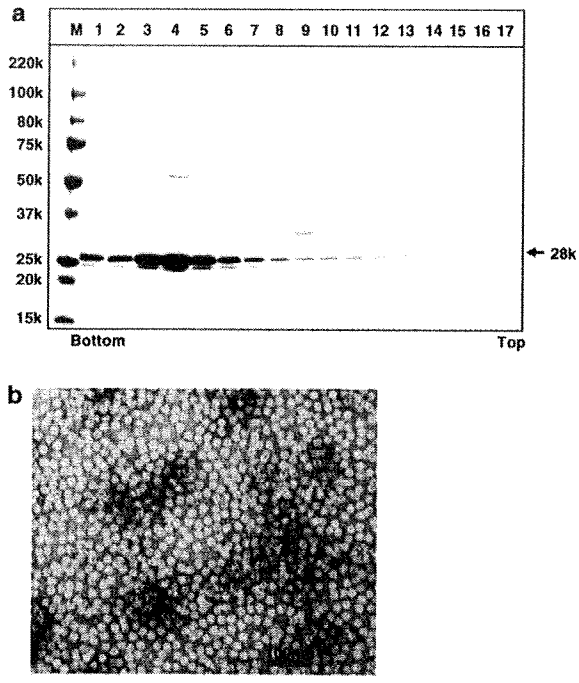

Fig. 2 **a** Purification PCV2-LPs by CsCl gradient centrifugation. The supernatant of the recombinant baculovirus-infected Tn5 cells was centrifuged for 3 h at 31,000 rpm in a Beckman SW32Ti rotor. The pellet was resuspended in 4.5 ml ExCell 405 and mixed with 2.1 g CsCl, then centrifuged for 24 h at 35,000 rpm in an SW55Ti rotor. Aliquots from the gradient were analyzed by electrophoresis on a 5–20% polyacrylamide gel and stained with Coomassie blue. The bottom and top of the gradient and the positions of molecular weight standards are indicated. **b** Electron microscopy of PCV2-LPs. Purified PCV2-LPs were stained with 2% uranyl acetate and observed by EM. *Bar* 100 nm

swine serum samples was collected from a slaughterhouse in Japan in 2006. All of the serum samples were diluted 1:200 for the ELISA test. The result showed that all sera from healthy slaughtered domestic pigs were positive for IgG against PCV2, and the OD values were above 0.65 without exception (data not shown).

Antibodies to the PCV2-LPs were prepared in rabbits and guinea pigs by subcutaneous injection of the purified PCV2-LPs. After being injected two times, the animals produced high levels of IgG antibodies, and the titers reached levels as high as 1:1,638,400 in the antibody ELISA. Immunogenicity of the VLPs was examined using an ELISA with rabbit and guinea pig hyperimmune sera as the capture and detector antibodies, respectively. As shown in Fig. 3b, the sensitivity reached 0.16 ng/ml of PCV2-LPs when a cutoff OD value of 0.2 was used, and native PCV2 particles were detected in the culture medium of PCV2-infected PK-15 cells, yielding an antigen titer of 1:32. Native PCV2 particles concentrated by centrifugation (100,000×*g*, 2 h) showed an increased titer of 1:256 (data not shown). These results demonstrated that the PCV2-LPs were immunogenic and able to elicit antibodies capable of binding to native PCV2 particles.

PCV2 is a pivotal causative agent of PMWS and is recognized as a major economic problem in the porcine industry worldwide [2, 10, 12, 26]. In addition, PCV2 infection is subclinical in some swine, and these swine become carriers and cause longer virus circulation in herds. However, the development of a vaccine and diagnosis are hampered by a low yield of PCV2 in cell culture. PCV2 capsid protein is the major structural protein and is highly

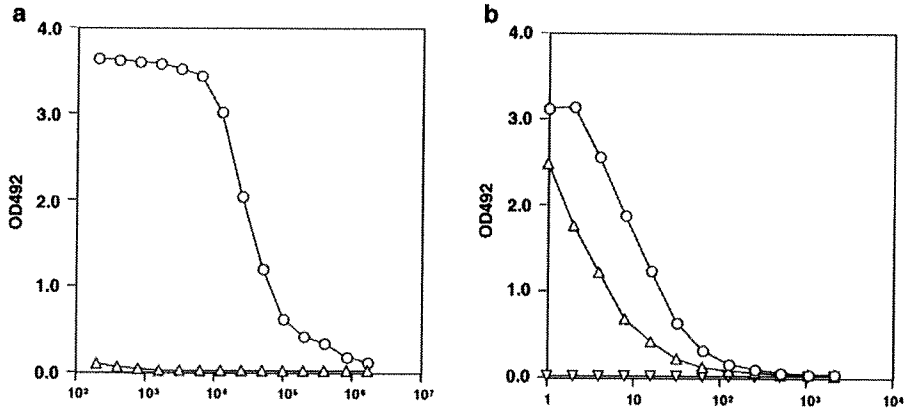

Fig. 3 **a** Antigenicity of PCV2-LPs. A swine was experimentally infected. The pre-serum was obtained before PCV2 infection, and the post-serum was obtained 4 weeks after infection. Both pre- (*open triangle*) and post-sera (*open circle*) were examined for IgG antibody by twofold dilutions starting from 1:200. **b** Immunogenicity of PCV2-LPs. Anti-PCV2-LP serum from a rabbit was used to coat a 96-well microplate. The binding of recombinant PCV2-LPs (10 ng/ml) (*open circle*) and native PCV2 particles produced in the supernatant of Yamagata-strain-infected PK-15 cells (*open triangle*) was examined by antigen ELISA. The OD value was considered positive when the absorbance was ≥0.150. The culture medium from uninfected PK-15 cells (*open inverted triangle*) was used as a negative control

immunogenic. As both neutralizing monoclonal antibodies and neutralizing swine sera have been shown to react with the capsid protein [13, 19, 24], the capsid protein is an attractive immunogen for vaccine development and diagnosis.

The recombinant baculovirus expression system has long been used to express proteins as well as to generate VLPs in various DNA and RNA viruses [3, 11, 14, 15, 18]. This system has many advantages over other systems: efficient expression, proper post-translational modification, correct conformation, and self-assembly of the capsid protein into VLPs, which usually retain the immunogenicity as well as physicochemical properties of their native virions. Sf9 and Tn5 cells are commonly used cell lines for the baculovirus expression system. Previous studies have shown that PCV2 capsid protein expressed in Sf9 cells self-assembled into VLPs [22]. However, although VLPs were generated in the Sf9 cells, they were not released into the culture medium. When we expressed the PCV2 capsid in Sf9 cells, the same result was observed. In contrast, when the recombinant PCV2 capsid protein was expressed in Tn5 cells, the capsid protein efficiently self-assembled into VLPs and, interestingly, was released into the culture medium, making purification of the VLPs easy. The yield of the purified VLPs reached 1 mg per 10^7 Tn5 cells, providing a virtually unlimited supply of highly purified PCV2-LPs.

The feasibility of the capsid protein-based PCV2 vaccine was demonstrated in several previous studies, where the successful induction of specific serum antibodies was observed [4, 9, 27]. It was also found that the absence of PCV2-neutralizing antibodies is well correlated with the virus replication and development of PMWS [21], indicating that the humoral immune response plays an important role in the prophylaxis of PCV2 infection. There are several advantages to using PCV2-LPs as a vaccine: First, the PCV2-LPs have an excellent safety profile, since there is no viral genome in the particles. Second, the PCV2-LPs have antigenicity and immunogenicity similar to those of the native PCV2. Third, the PCV2-LPs are morphologically the same as the native PCV2, and the conformational antigenic epitopes may be properly retained. Therefore, the PCV2-LPs share the same immunogenicity with the native PCV2 virion. In fact, antibodies elicited with PCV2-LPs strongly reacted with the native virion. These results clearly demonstrate that PCV2-LPs are a promising PCV2 vaccine candidate.

Acknowledgments The authors thank Tomoko Mizoguchi for secretarial work and Dr. Kenji Kawashima (National Institute of Animal Health, Japan) for kindly supplying rabbit antiserum to PCV2. This study was supported in part by grants for Research on Emerging and Re-emerging Infectious Diseases, Research on Hepatitis, and Research on Food Safety from the Ministry of Health, Labor, and Welfare, Japan. This study was also supported in part by the Japan-China Sasakawa Medical Fellowship.

References

1. Allan GM, Ellis JA (2000) Porcine circoviruses: a review. J Vet Diagn Invest 12:3–14
2. Allan GM, Mc Neilly F, Meehan BM, Kennedy S, Mackie DP, Ellis JA, Clark EG, Espuna E, Saubi N, Riera P, Botner A, Charreyre CE (1999) Isolation and characterisation of circoviruses from pigs with wasting syndromes in Spain, Denmark and Northern Ireland. Vet Microbiol 66:115–123
3. Baumert TF, Vergalla J, Satoi J, Thomson M, Lechmann M, Herion D, Greenberg HB, Ito S, Liang TJ (1999) Hepatitis C virus-like particles synthesized in insect cells as a potential vaccine candidate. Gastroenterology 117:1397–1407
4. Blanchard P, Mahe D, Cariolet R, Keranflec'h A, Baudouard MA, Cordioli P, Albina E, Jestin A (2003) Protection of swine against post-weaning multisystemic wasting syndrome (PMWS) by porcine circovirus type 2 (PCV2) proteins. Vaccine 21:4565–4575
5. Ellis J, Hassard L, Clark E, Harding J, Allan G, Willson P, Strokappe J, Martin K, McNeilly F, Meehan B, Todd D, Haines D (1998) Isolation of circovirus from lesions of pigs with post-weaning multisystemic wasting syndrome. Can Vet J 39:44–51
6. Ellis J, Krakowka S, Lairmore M, Haines D, Bratanich A, Clark E, Allan G, Konoby C, Hassard L, Meehan B, Martin K, Harding J, Kennedy S, McNeilly F (1999) Reproduction of lesions of postweaning multisystemic wasting syndrome in gnotobiotic piglets. J Vet Diagn Invest 11:3–14
7. Ellis JA, Bratanich A, Clark EG, Allan G, Meehan B, Haines DM, Harding J, West KH, Krakowka S, Konoby C, Hassard L, Martin K, McNeilly F (2000) Coinfection by porcine circoviruses and porcine parvovirus in pigs with naturally acquired post-weaning multisystemic wasting syndrome. J Vet Diagn Invest 12:21–27
8. Fenaux M, Halbur PG, Gill M, Toth TE, Meng XJ (2000) Genetic characterization of type 2 porcine circovirus (PCV-2) from pigs with postweaning multisystemic wasting syndrome in different geographic regions of North America and development of a differential PCR-restriction fragment length polymorphism assay to detect and differentiate between infections with PCV-1 and PCV-2. J Clin Microbiol 38:2494–2503
9. Fenaux M, Opriessnig T, Halbur PG, Elvinger F, Meng XJ (2004) A chimeric porcine circovirus (PCV) with the immunogenic capsid gene of the pathogenic PCV type 2 (PCV2) cloned into the genomic backbone of the nonpathogenic PCV1 induces protective immunity against PCV2 infection in pigs. J Virol 78:6297–6303
10. Hasslung F, Wallgren P, Ladekjaer-Hansen AS, Botner A, Nielsen J, Wattrang E, Allan GM, McNeilly F, Ellis J, Timmusk S, Belak K, Segall T, Melin L, Berg M, Fossum C (2005) Experimental reproduction of postweaning multisystemic wasting syndrome (PMWS) in pigs in Sweden and Denmark with a Swedish isolate of porcine circovirus type 2. Vet Microbiol 106:49–60
11. Ishii Y, Ozaki S, Tanaka K, Kanda T (2005) Human papillomavirus 16 minor capsid protein L2 helps capsomeres assemble independently of intercapsomeric disulfide bonding. Virus Genes 31:321–328
12. Kim J, Chung HK, Jung T, Cho WS, Choi C, Chae C (2002) Postweaning multisystemic wasting syndrome of pigs in Korea: prevalence, microscopic lesions and coexisting microorganisms. J Vet Med Sci 64:57–62
13. Lekcharoensuk P, Morozov I, Paul PS, Thangthumniyom N, Wajjawalku W, Meng XJ (2004) Epitope mapping of the major

capsid protein of type 2 porcine circovirus (PCV2) by using chimeric PCV1 and PCV2. J Virol 78:8135–8145
14. Li TC, Yamakawa Y, Suzuki K, Tatsumi M, Razak MA, Uchida T, Takeda N, Miyamura T (1997) Expression and self-assembly of empty virus-like particles of hepatitis E virus. J Virol 71:7207–7213
15. Li TC, Takeda N, Kato K, Nilsson J, Xing L, Haag L, Cheng RH, Miyamura T (2003) Characterization of self-assembled virus-like particles of human polyomavirus BK generated by recombinant baculoviruses. Virology 311:115–124
16. Li TC, Takeda N, Miyamura T, Matsuura Y, Wang JC, Engvall H, Hammar L, Xing L, Cheng RH (2005) Essential elements of the capsid protein for self-assembly into empty virus-like particles of hepatitis E virus. J Virol 79:12999–13006
17. Mahe D, Blanchard P, Truong C, Arnauld C, Le Cann P, Cariolet R, Madec F, Albina E, Jestin A (2000) Differential recognition of ORF2 protein from type 1 and type 2 porcine circoviruses and identification of immunorelevant epitopes. J Gen Virol 81:1815–1824
18. Matsuo E, Tani H, Lim C, Komoda Y, Okamoto T, Miyamoto H, Moriishi K, Yagi S, Patel AH, Miyamura T, Matsuura Y (2006) Characterization of HCV-like particles produced in a human hepatoma cell line by a recombinant baculovirus. Biochem Biophys Res Commun 340:200–208
19. McNeilly F, McNair I, Mackie DP, Meehan BM, Kennedy S, Moffett D, Ellis J, Krakowka S, Allan GM (2001) Production, characterisation and applications of monoclonal antibodies to porcine circovirus 2. Arch Virol 146:909–922
20. Meehan BM, McNeilly F, Todd D, Kennedy S, Jewhurst VA, Ellis JA, Hassard LE, Clark EG, Haines DM, Allan GM (1998) Characterization of novel circovirus DNAs associated with wasting syndromes in pigs. J Gen Virol 79(Pt 9):2171–2179
21. Meerts P, Misinzo G, Lefebvre D, Nielsen J, Botner A, Kristensen CS, Nauwynck HJ (2006) Correlation between the presence of neutralizing antibodies against porcine circovirus 2 (PCV2) and protection against replication of the virus and development of PCV2-associated disease. BMC Vet Res 2:6
22. Nawagitgul P, Morozov I, Bolin SR, Harms PA, Sorden SD, Paul PS (2000) Open reading frame 2 of porcine circovirus type 2 encodes a major capsid protein. J Gen Virol 81:2281–2287
23. Onuki A, Abe K, Togashi K, Kawashima K, Taneichi A, Tsunemitsu H (1999) Detection of porcine circovirus from lesions of a pig with wasting disease in Japan. J Vet Med Sci 61:1119–1123
24. Pogranichnyy RM, Yoon KJ, Harms PA, Swenson SL, Zimmerman JJ, Sorden SD (2000) Characterization of immune response of young pigs to porcine circovirus type 2 infection. Viral Immunol 13:143–153
25. Pringle CR (1999) Virus taxonomy-1999. The universal system of virus taxonomy, updated to include the new proposals ratified by the International Committee on Taxonomy of Viruses during 1998. Arch Virol 144:421–429
26. Rodriguez-Arrioja GM, Segales J, Calsamiglia M, Resendes AR, Balasch M, Plana-Duran J, Casal J, Domingo M (2002) Dynamics of porcine circovirus type 2 infection in a herd of pigs with postweaning multisystemic wasting syndrome. Am J Vet Res 63:354–357
27. Wang X, Jiang P, Li Y, Jiang W, Dong X (2007) Protection of pigs against post-weaning multisystemic wasting syndrome by a recombinant adenovirus expressing the capsid protein of porcine circovirus type 2. Vet Microbiol 121:215–224

Biological and immunological characteristics of hepatitis E virus-like particles based on the crystal structure

Tetsuo Yamashita[a,1], Yoshio Mori[a,1], Naoyuki Miyazaki[b,c], R. Holland Cheng[c], Masato Yoshimura[d], Hideaki Unno[e], Ryoichi Shima[a], Kohji Moriishi[a], Tomitake Tsukihara[b], Tian Cheng Li[f], Naokazu Takeda[f], Tatsuo Miyamura[f], and Yoshiharu Matsuura[a,2]

[a]Department of Molecular Virology, Research Institute for Microbial Diseases and [b]Department of Protein Crystallography, Research Institute for Protein Research, Osaka University, Osaka 565-0871, Japan; [c]Department of Molecular and Cellular Biology, University of California, Davis, CA 95616; [d]National Synchrotron Radiation Research Center, 101 Hsin-Ann Road, Hsinchu Science Park, Hsinchu 30076, Taiwan; [e]Department of Applied Chemistry, Faculty of Engineering, Nagasaki University, Nagasaki 852-8521, Japan; and [f]Department of Virology II, National Institute of Infectious Diseases, Tokyo 208-0011, Japan

Edited by Michael G. Rossmann, Purdue University, West Lafayette, IN, and approved June 8, 2009 (received for review April 3, 2009)

Hepatitis E virus (HEV) is a causative agent of acute hepatitis. The crystal structure of HEV-like particles (HEV-LP) consisting of capsid protein was determined at 3.5-Å resolution. The capsid protein exhibited a quite different folding at the protruding and middle domains from the members of the families of *Caliciviridae* and *Tombusviridae*, while the shell domain shared the common folding. Tyr-288 at the 5-fold axis plays key roles in the assembly of HEV-LP, and aromatic amino acid residues are well conserved among the structurally related viruses. Mutational analyses indicated that the protruding domain is involved in the binding to the cells susceptive to HEV infection and has some neutralization epitopes. These structural and biological findings are important for understanding the molecular mechanisms of assembly and entry of HEV and also provide clues in the development of preventive and prophylactic measures for hepatitis E.

capsid | HEV | VLP

Hepatitis E is an acute viral hepatitis caused by infection with hepatitis E virus (HEV) that is transmitted primarily by a fecal-oral route (1, 2). Numerous epidemic and sporadic cases have occurred in developing countries of Asia, the Middle East, and North Africa, where sanitary conditions are not well-maintained. Hepatitis E affects predominantly young adults, and HEV infection in pregnancy is one of the risk factors for severe disease and death (3). Recent epidemiological studies show that significant prevalence of HEV and anti-HEV antibody is found in humans and several animals worldwide, even in developed countries (4–8).

HEV is the sole member of the genus *Hepevirus* within the family *Hepeviridae* and has a 7.2-kb positive-sense RNA genome (9). Five major genotypes have been identified so far (2). The viruses in the genotypes 1 and 2 are maintained among only humans, while those in the genotypes 3 and 4 are found in pigs or wild animals (4–6). However, infections of human with genotypes 3 and 4 via zoonotic transmission or blood transfusion were reported in the developed countries, such as Japan and the United States (7, 8, 10), suggesting that hepatitis E caused by infection with genotypes 3 and 4 of HEV is an important emerging infectious disease. The viruses in the genotype 5 are of avian origin and are thought to be uninfectious to humans (11). The genomic RNA contains three ORFs (ORFs) encoding nonstructural proteins (ORF1), the viral capsid protein composed of 660 amino acids (ORF2) and a small phosphorylated protein of unidentified function (ORF3) (1, 9). The viral capsid protein induces neutralizing antibodies by its immunization (12–15) or during the course of infection (16, 17). A typical signal sequence at the N terminus and 3 potential *N*-glycosylation sites (Asn-X-Ser/Thr) are well-conserved in the capsid protein derived from all mammalian genotypes (18, 19), but the glycosylation status of this protein is still controversial and the biological significance of the modification in the viral life cycle remains unknown. Although propagation of HEV in the cell culture systems reported in earlier studies was not efficient (20–23), Tanaka et al. succeeded in the establishment of a persistent infection system of HEV genotype 3 in human hepatoma (PLC/PRF/5) and human carcinomic alveolar epithelial (A549) cell lines (24). However, sufficient amounts of viral particles cannot be obtained for studies of the structure, life cycle, and pathogenesis of HEV.

Electron microscopy of human stool specimens showed that HEV is a nonenveloped spherical particle with a diameter of approximately 320 Å (25). As an alternative to in vitro propagation of HEV, the baculovirus expression system opens the prospect of studying HEV capsid assembly, since HEV-like particles (HEV-LP) with protruding spikes on the surface can be formed in insect cells infected with a recombinant baculovirus expressing the capsid protein of a genotype 1 strain (26–28). Cryo-electron microscopic (cryoEM) analysis has revealed that HEV-LP is a $T = 1$ icosahedral particle composed of 60 copies of truncated products of ORF2 (27, 28). The HEV-LP appeared to be empty due to a lack of significant density containing RNA inside and was 270 Å in diameter (26–28), which is smaller than the diameter of the native virions. However, the HEV-LP retained the antigenicity and capsid formation of the native HEV particles.

The crystal structures of the recombinant or native $T = 3$ viral particles derived from structurally related mammalian and plant viruses, such as recombinant Norwalk virus (rNV; PDB accession code 1IHM) (29), San Miguel sea lion virus (SMSV; PDB accession code 2GH8) (30), the members of the family *Caliciviridae*, and Carnation mottle virus (CARMV; PDB accession code 1OPO) (31), a member of the family *Tombusviridae*, have

Author contributions: T.Y., Y. Mori, T.T., T.C.L., N.T., T.M., and Y. Matsuura designed research; T.Y., Y. Mori, R.S., K.M., T.C.L., N.T., and Y. Matsuura performed research; T.Y., Y. Mori, N.M., R.H.C., M.Y., and H.U. analyzed data; and T.Y., Y. Mori, and Y. Matsuura wrote the paper.

The authors declare no conflict of interest.

This article is a PNAS Direct Submission.

Data deposition: The atomic coordinates have been deposited in the Protein Data Bank, www.pdb.org (PDB ID code 2ZTN).

[1]T.Y. and Y. Mori contributed equally to this work.

[2]To whom correspondence should be addressed at: Department of Molecular Virology, Research Institute for Microbial Diseases, Osaka University, 3-1 Yamadaoka, Suita-shi, Osaka 565-0871, Japan. E-mail: matsuura@biken.osaka-u.ac.jp.

This article contains supporting information online at www.pnas.org/cgi/content/full/0903699106/DCSupplemental.

www.pnas.org/cgi/doi/10.1073/pnas.0903699106

been determined at resolutions of 3.4 Å, 3.2 Å, and 3.2 Å, respectively. In this study, to understand the structural basis on HEV, we solved the crystal structure of HEV-LP derived from a genotype 3 strain at 3.5-Å resolution and found differences in the folding of the capsid protein among these viruses. On the other hand, we found several structural similarities of shell formation. In particular, it was revealed that aromatic amino acids (Tyr-288 in the case of HEV-LP) at the 5-fold axis play a crucial role in the hydrophobic interaction required for particle formation and are well conserved among these viruses. Furthermore, mutational analyses depicted the putative cellular receptor-binding regions and epitopes for neutralizing of binding (NOB) antibodies on the 3D structure of HEV-LP. The availability of the 3D structure of HEV-LP at high resolution will provide valuable information not only for analyses of the entry and assembly of HEV, but also for the development of a vaccine for hepatitis E.

Results

Preparation of HEV-LP of a Genotype 3. Upon infection with a recombinant baculovirus possessing a genome of the truncated capsid protein (amino acids 112–608) from a genotype 3 strain under the control of polyhedrin promoter, a large amount of HEV-LP was secreted into the culture supernatant as described in the case of HEV-LP of genotype 1 strain (26–28). The purified HEV-LP of genotype 3 was used for further structural and biological analyses.

Overall Structure of HEV-LP. The crystal structure of HEV-LP derived from the genotype 3 strain was determined at 3.5-Å resolution by the molecular replacement method by using a cryoEM map of HEV-LP derived from the genotype 1 strain (27, 28) as an initial phasing model (Fig. 1*A*). As shown in the previous papers (27, 28), HEV-LP shows a $T = 1$ icosahedral symmetry with an external diameter of 270 Å. This particle is composed of 60 subunits of the truncated capsid proteins, forming the icosahedral 2-, 3-, and 5-fold axes. It has 30 protrusions at the 2-fold axis of the surface with large depressions at the 3- and 5-fold axes.

Structure of the HEV Capsid Protein. The truncated HEV capsid protein has 3 definite domains designated as S (shell), M (middle), and P (protruding) composed of the amino acid residues 129–319, 320–455, and 456–606, respectively (Fig. 1*B*). Because the N- and C-terminally truncated capsid proteins were used for the characterization, the typical signal sequence (amino acids 1–22) and following arginine-rich domain (amino acids 23–111) and the C-terminal domain removed by cleavage in insect cells (amino acids 609–660) were not determined in this study. Additionally, the amino acid residues 112–128, 486–487, 555–560, and 607–608 were disordered in this study. The S domain, which forms an internal scaffold structure of the particle, folds into a classical anti-parallel jelly roll-like β-sandwich structure with 8 β-strands (designated as B to I) and 4 short α-helices that are conserved among many viral capsids (Fig. 1*B* and Fig. S1) (29–33). The M domain, which is one of the characteristic domains, has a twisted anti-parallel β-barrel structure composed of 6 β-strands and 4 short α-helices. This domain is tightly associated with the S domain and located on the surface around the icosahedral 3-fold axis (Fig. 1*A* and *B*). The M and P domains are linked with a long proline-rich hinge (amino acids 445–467). Previous studies on the structures of rNV (29) and SMSV (30) revealed that the P domains of the viruses are composed of 2 subdomains, P1 and P2, and the P2 subdomain is located as a large protrusion of the P1 subdomain (Fig. S1). In contrast, the P domain of HEV-LP is composed of a single individual domain forming a twisted anti-parallel β-sheets structure (Fig. 1*B* and Fig. S1), demonstrating that the capsid protein

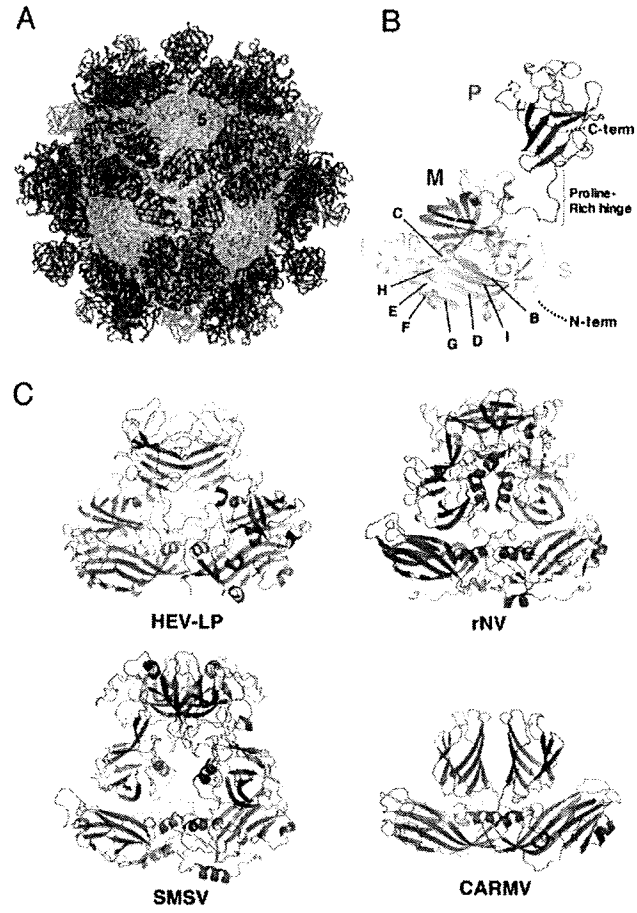

Fig. 1. Crystal structure of HEV-LP and comparison of capsid protein dimers of HEV-LP, rNV, SMSV, and CARMV. The S, M, and P domains of the HEV capsid protein are indicated by pink, green, and blue, respectively. (*A*) HEV-LP is composed of sixty capsid subunits forming icosahedral 2-, 3-, and 5-fold axes and indicating a $T = 1$ symmetry. (*B*) The ribbon diagram of a capsid subunit of HEV-LP (PDB accession code: 2ZTN) shows P, M, and S domains at the top, middle, and bottom, respectively. The disordered regions are shown with dashed lines. The S domain shows a jerry roll-like β-barrel structure conserved in some viruses. The conserved anti-parallel β-strands are indicated (B to I). (*C*) The ribbon diagrams of crystal structures of capsid protein dimers of HEV-LP and those of rNV (PDB accession code 1IHM), SMSV (PDB accession code 2GH8), and CARMV (PDB accession code 1OPO) are indicated. Each capsid protein monomer is colored in red and blue.

of HEV-LP has a significantly different fold from those of caliciviruses, except for the S domain. Although we have no evidence of glycosylation of HEV-LP prepared in insect cells, the HEV capsid protein has 3 potential *N*-glycosylation sites, Asn-137-Leu-Ser, Asn-310-Leu-Thr and Asn-562-Thr-Thr (19). In the dimer structure, the former 2 sites are mapped on the horizontal surface of the S domain, as shown in Fig. S2*A*. However, Asn-137 and Asn-310 are located in the interfaces of the pentamer and trimer structures, respectively (Fig. S2*B* and *C*), suggesting that, if it occurs at all, *N*-glycosylation in these sites may inhibit assembly of HEV-LP. Indeed, Graff et al. (18) reported that HEV carrying mutations in Asn-137 or Asn-310 to Glu lost infectivity to cells or rhesus macaques due to a defect in the virion assembly. On the other hand, Asn-562 is mapped in the central region in the top of the P dimer and exposed in the surface of HEV-LP.

The Dimer Structure at the 2-Fold Axis. It is noteworthy that the HEV-LP dimer at the icosahedral 2-fold axis shows a crossing

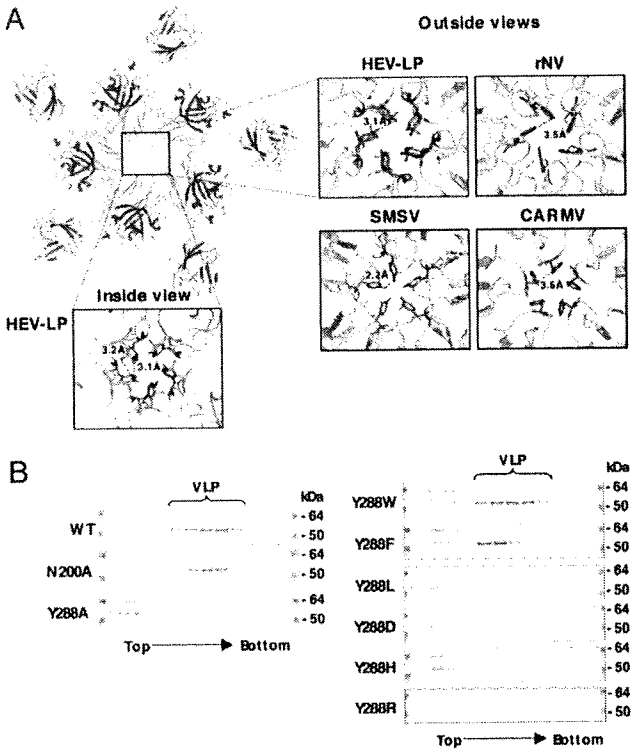

Fig. 2. Interaction of capsid protein subunits of HEV-LP around the 5-fold axis. (*A*) The pentamer of the capsid protein of HEV-LP. The close-up surface diagram of the 5-fold axis showed from outside and inside of HEV-LP. Amino acid residues Asn-200 and Tyr-288 are shown in yellow and green, respectively. The close-up surface diagram of the 5-fold axis showed from outside of rNV, SMSV, and CARMV. The aromatic amino acids Phe-118 of rNV, Tyr-330 of SMSV, and Phe-145 of CARMV are indicated in green. The deduced interacting atoms are connected with dashed lines, and the distances are indicated. (*B*) Sucrose density fractionation assay using the wild-type or mutant capsid proteins (53 kDa) in which the amino acids composing the 5-fold axis were substituted. The capsid protein composing HEV-LP was found in the 5–9th fractions from the top, while that which failed to form particles was found in the top fractions. The molecular mass of approximately 64 kDa was a non-specific protein.

topology of the P versus M and S domains, while that of the other viruses with protrusions at the 2-fold axis, containing rNV, SMSV, and CARMV, exhibits a parallel topology of each domain (Fig. 1*C*). The flexibility of the long proline-rich hinge region between the M and P domains allows this unique topology of HEV-LP. The P domain of HEV-LP interacts with not only the P domain but also the M domain of the counterpart to stabilize the dimer structure. Despite these topological differences, the overall structure of the protrusion dimeric structure at the 2-fold axis is similar to that of rNV and SMSV. The disordered residues 486–487 and 555–560 are located in the apical region of the protrusion, suggesting that this region is flexible to take advantage of the interaction with other molecules.

Five-Fold Axis Packaging. The inter-molecule-interface of the capsid pentamer at the icosahedral 5-fold axis is composed of only S domains, and these interaction regions are narrower than those of the dimer and trimer at the 2-fold and 3-fold axes, respectively (Fig. 2*A*), suggesting that the pentamer formation is a key step of HEV-LP assembly. There are 4 loops between the β-sheets in the S domain, designated as loops B–C (amino acids 139–152), D–E (amino acids 196–206), F–G (amino acids 236–241), and H–I (amino acids 281–296), around the center of the pentamer structure. Among them, the loops B–C and F–G are not in close proximity to the next subunits, suggesting they are not implicated in the inter-molecular interaction. In contrast, loops D–E and H–I do interact with the next subunits. In particular, the side chains of Asn-200 and Tyr-288 in loops D–E and H–I, respectively, interact with those of the next subunits, from which they are separated by a distance of approximately 3.2 Å, filling in the central pore (Fig. 2*A*). These observations led us to hypothesize that these amino acid residues are important for assembly and stability of the particles. To examine this hypothesis, we constructed 2 mutant capsid proteins in which Asn-200 was replaced with alanine (N200A) or Tyr-288 was replaced with alanine (Y288A), and the effect of these mutations on the particle formation was determined by a density-fractionation assay (Fig. 2*B*). Comparative amounts of the mutant proteins to the wild-type capsid were expressed and released into the supernatants of cells infected with the recombinant baculoviruses. N200A but not Y288A formed VLP as the wild-type, indicating that Tyr-288 plays a more crucial role in particle formation than Asn-200. The aromatic amino acids, Phe-118, Tyr-330, and Phe-145, are also found in the icosahedral 5-fold axis of rNV, SMSV, and CARMV, respectively (Fig. 2*A*). To examine the role of the aromatic side chain in Tyr-288 in the particle formation, a series of mutants in which Tyr-288 was replaced with tryptophan, phenylalanine, leucine, asparatic acid, histidine, or arginine (Y288W, Y288F, Y288L, Y288D, Y288H, or Y288R) were generated. All of them were expressed and released into the culture medium, as well as was the wild type. The mutants with aromatic amino acids, Y288W and Y288F, were able to form HEV-LP, whereas other mutants produced no or very few particles (Fig. 2*B*). These results suggest that the aromatic side chain of Tyr-288 plays a crucial role in the HEV-LP formation by shutting off the central pore of the pentamer, and that the aromatic amino acids in the positions corresponding to Tyr-288 of HEV are functionally conserved among the structurally related viruses.

Binding of HEV-LP to Cultured Cells. The early steps of HEV entry remain unclear because of the lack of a robust cell culture system for HEV, despite recent progress in the in vitro propagation of HEV in the cell lines PLC/PRF/5 and A549 (24). HEV-LP was able to bind to several cell lines, including PLC/PRF/5 and A549 cells, but not to mouse myeloma P3 × 63Ag8U.1 (P3U1) cells (Fig. S3), suggesting that a binding assay using HEV-LP is useful to examine the first step of receptor-binding of HEV to the target cells. Among the cell lines examined, the human hepatoma cell line Huh7, exhibited a greater ability to bind to HEV-LP than the cell lines PLC/PRF/5 and A549. Therefore, Huh7 cells were used for the following binding experiments of HEV-LP.

Three-Dimensional Mapping of Epitopes for NOB Antibodies. We examined the ability of the 10 newly produced anti-HEV-LP monoclonal antibodies to inhibit the binding of HEV-LP to Huh7 cells (Fig. 3*A*). Two of the monoclonal antibodies, MAB1323 and MAB272, exhibited NOB of HEV-LP to Huh7 cells and recognized the P domain by immunoblotting using the GST (GST)-fused HEV capsid proteins (Fig. S4). However, further truncation of the C-terminal 28 or N-terminal 24 amino acids from the GST-fused P domain abrogated the binding with the antibodies, indicating that it is difficult to determine the epitopes of the antibodies in more detail using a series of truncated mutants of the P domain. A competitive enzyme-linked immunosorbent assay (ELISA) suggested that MAB1323, MAB272, and MAB161, but not MAB358, which was used as a detector in the binding assay, recognized the same or adjacent epitopes (Fig. S5). The P domains of rNV and feline calicivirus were suggested to be involved in the binding to the receptor molecules (34–36), and we therefore hypothesized that the P

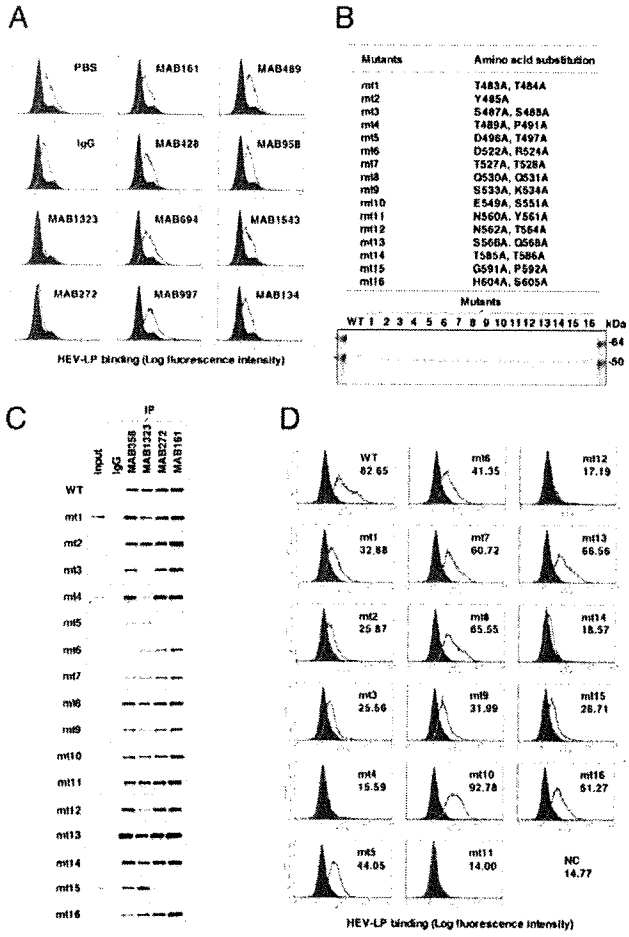

Fig. 3. Characterization of monoclonal antibodies and mutant HEV-LPs. (*A*) Neutralization of binding (NOB) of HEV-LP to Huh7 cells by monoclonal antibodies to HEV-LP. After preincubation of HEV-LP (10 μg/mL) with each of the monoclonal antibodies (20 μg/mL) for 1 h at 37°C, the mixture was inoculated into Huh7 cells and incubated for 1 h at 4°C. HEV-LP (lined area) bound to cells was detected by flow cytometry. The filled area indicates mock-incubated cells. (*B*) Construction of HEV-LP mutants. Sixteen HEV-LP mutants, in which the surface amino acid residues of the P domain were substituted, were constructed. The protein bands of 100 ng each of the purified wild-type and mutant HEV-LPs were visualized by Coomassie brilliant blue staining after SDS/PAGE. (*C*) Reactivities of NOB antibodies with the mutant HEV-LPs. Immunoprecipitation analyses of a series of HEV-LPs by NOB (MAB1323 and MAB272) or non-NOB antibodies (MAB358 and MAB161). Immunoprecipitated HEV-LPs were detected by an anti-HEV capsid rabbit polyclonal antibody. (*D*) Binding capability of the mutant HEV-LPs to Huh7 cells. Wild-type or mutant HEV-LPs (10 μg/mL) were incubated with Huh7 cells for 1 h at 4°C, and then HEV-LP (lined area) bound to cells was detected by flow cytometry. The filled area indicates mock-incubated cells. The MFI is shown in each panel.

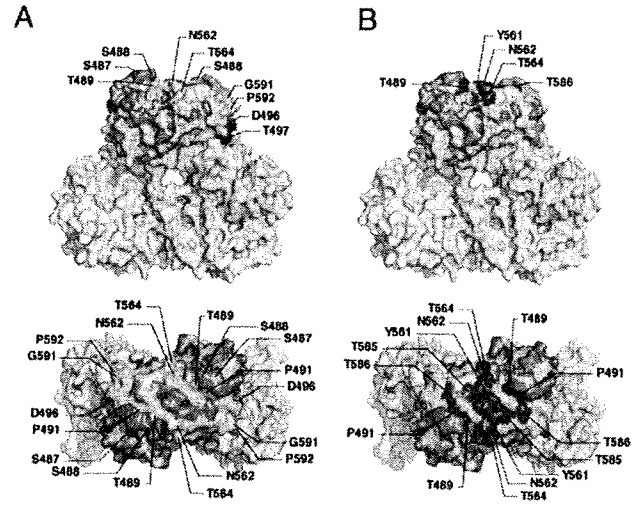

Fig. 4. Amino acid residues involved in the recognition by NOB antibodies and in the binding to Huh7 cells. Surface diagrams of the capsid protein dimer from a lateral (*Upper*) or top (*Lower*) view. (*A*) Amino acids in HEV-LP involved in the complete loss (deep color) or reduction (light color) of reactivity to MAB1323 and MAB272 are shown in orange and green, respectively. (*B*) Amino acids in HEV-LP responsible for binding to Huh7 cells are shown in red. Domains S, M, and P are colored pink, blue and gray, respectively. The substitutions in the P domain of HEV-LP that exhibited no effect on the reactivity with NOB antibodies or the binding to Huh7 cells are shown in dark gray.

domain of HEV-LP might also be involved in the cell binding. To examine this possibility, we prepared 16 HEV-LP mutants in which 1 or 2 amino acid residues at the surface of the P domain were substituted (Fig. 3*B*). The density fractionation assay indicated that all of the mutant proteins formed HEV-LP in the manner of the wild-type capsid protein. MAB358, which recognized an epitope on the M domain (Fig. S4), was capable of precipitating all of the mutants (Fig. 3*C*). MAB1323 exhibited no interaction with mt3 and a weak precipitation of mt4 and mt12. Both MAB272 and MAB161 exhibited no or weak precipitation of mt5 and mt15, whereas MAB272 but not MAB161 exhibited NOB of HEV-LP to Huh7 cells (Fig. 3*A* and *C*). The substituted amino acids of these mutants are illustrated in the 3D structure of the capsid dimer (Fig. 4*A*), and these results suggest that the NOB antibodies MAB1323 and MAB272 recognize the peripheral region of the apical surface (orange) and the horizontal region (green) of the P domain above the M domain at the 3-fold axis, respectively.

Three-Dimensional Mapping of a Region Crucial for Binding to the Target Cells. To determine the region important for binding to the cell surface, the mutant HEV-LPs substituted into the P domain were also used in the assay of binding to Huh7 cells (Fig. 3*D*). The wild-type HEV-LP bound to Huh7 cells with a geographic mean fluorescence intensity (MFI) of 82.65. Among the mutants examined, mt4, mt11, mt12, and mt14 exhibited significantly low MFI values of less than 20. Similar results were obtained using A549 cells (Fig. S6). The amino acid residues required for cell binding were mapped in the central flexible region of the apical surface as shown in Fig. 4*B* (red). This region is partially overlapped with epitopes of MAB1323 (Fig. 4*A*) and other neutralizing antibodies reported by Schofield et al. (16) as shown in Fig. S7. These results suggested that the apical center region of the P domain is involved in the association with not-yet-identified cellular receptor(s).

Discussion

The expression of the truncated HEV capsid protein (amino acids 112–608) in insect cells resulted in assembly of HEV-LP, which retains an antigenicity similar to that of the native HEV particles (26, 37). This particle with a $T = 1$ symmetry has a diameter of 270 Å, which is smaller than the 320-Å diameter of the native virion detected in the fecal specimens of patients (25). It has been reported that the interior cavity of HEV-LP is too small to accommodate a viral RNA of 7.8 kb in length (28) and that the particles show no evidence of nucleotide contents (26, 28). Therefore, native HEV particles are sug-

Table 1. Data collection and processing statistics for HEV-LP

Data collection	
Space group	$P2_12_12_1$
Cell dimensions	
a, *b*, *c*, Å	336.8, 349.4, 359.5
X-ray wavelength, Å	1.0000
Resolution, Å	50–3.55 (3.68–3.55)
R_{merge}*	0.131 (0.498)
$I/\sigma I$	9.8 (3.2)
Completeness, %	99.9 (99.8)
Redundancy	5.6 (5.2)
Refinement	
Resolution range, Å	20–3.56
No. reflections	494,466
R_{work}/R_{free}	30.5/30.9
No. atoms	
Protein	215,400
B factors	
Protein	94.9
rmsd	
Bond length, Å	0.009
Bond angle, °	1.355

Values in square brackets refer to the highest-resolution shell.
*$R_{merge} = \Sigma_{hkl}\Sigma_i|I(hkl)_i - \langle I(hkl)\rangle|/\Sigma_{hkl}I(hkl)$, where $I(hkl)_i$ is the *i*th measurement of the intensity of reflection hkl and $\langle I(hkl)\rangle$ is the mean intensity of reflection *hkl*.

gested to be composed of a larger number and/or a larger size of capsid proteins than HEV-LP. In some cases of plant viruses with a $T = 3$ symmetry, the capsid proteins assembled into particles with a $T = 1$ symmetry by deletion of the N-terminal basic region (38, 39) or amino acid substitutions either in the N-terminal region or in the linker domain between the N-terminal region and S domain (39), suggesting that the N-terminal basic region plays an important role in switching of the transition from $T = 3$ to $T = 1$ symmetry. In addition, expression of the NV capsid protein in insect cells resulted in production of not only $T = 3$ large particles but also small particles thought to have the $T = 1$ symmetry (40). Based on many similarities of the capsid structures and their packaging of structurally related viruses, the native HEV particles are suggested to possess a $T = 3$ surface lattice. The flexibility of the proline-rich hinge linking the M and P domains could allow the capsid protein dimer to switch conformations between the A/B and C/C subunits found in $T = 3$ viruses. Although structure of the native HEV may be slightly different from that of the HEV-LP, the data obtained in this study by using HEV-LP should provide useful information to understand the structure of viral particle, life cycle, and pathogenesis of HEV. The S domain shares the jellyroll fold with some other icosahedral viruses (29–33). It was found that the capsid proteins with substitutions of Tyr-288 positioned at the center of the pentamer structure built in interS domain-interaction failed to assemble into HEV-LP. Alignment analysis of amino acid sequences using data available in GeneBank showed that Tyr-288 is completely conserved within 5 genotypes of HEV. Furthermore, residues corresponding to Tyr-288 of the HEV capsid protein are found in the structures of rNV (Phe-118), SMSV (Tyr-330), and CARMV (Phe-145), although the positions of these aromatic residues are different. Tyr-288 of HEV and Tyr-330 of SMSV located in the H-I loop and Phe-110 of rNV in the D–E loop are exposed at the outside surface of the particles, whereas Phe-145 of CARMV located in the D–E loop is exposed at the interior of the particle. These data suggest that the aromatic side chains of these residues are involved in hydrophobic interactions with those of the next subunits, assuring stable assembly of the particles. During entry into cells, rearrangement of the virion structure is required for release of the genome from the shell. However, the entry and uncoating mechanisms of HEV remain unknown. Because the center of the pentamer is the thinnest region of the particle and takes a channel-like structure (28), this region might also be important for uncoating and release of the viral RNA. It has been proposed that the 5-fold axis of poliovirus is involved in the genomic RNA translocation via conformational change of the virion initiated by binding to the receptor molecules (41, 42).

The first step in viral entry into a target cell is binding to the cellular receptors. The human hepatoma PLC/PRF/5 and lung epithelial A549 cell lines, which are highly susceptible to persistent HEV-infection (24), are likely to express functional HEV receptors on the cell surface. However, HEV-LP had reduced binding to these cells compared to the other cell lines examined. Therefore, the human hepatoma cell line Huh7, which also exhibited a susceptibility to HEV infection (13, 18) and readily bound to HEV-LP, was mainly used in this study. It has been reported that the P domains of noroviruses and the feline calicivirus were involved in the binding to the putative receptors, histo-blood antigens (35, 36) and the feline junctional adhesion molecule (34), respectively. The peptide of the HEV capsid protein (amino acids 368–606), which consists of a part of the M and an entire P domain, was shown to be capable of binding to several cell lines (13), suggesting that the P domain of HEV is also involved in the binding to the cell receptors. Indeed, the mutational analyses in this study indicated that the central flexible region of the top of the P domain of HEV-LP plays a crucial role for binding to Huh7 and A549 cells. This is consistent with a recent study by Graff et al. in which an N562Q mutant of HEV lost infectivity to culture cells and rhesus macaques despite the production of viral particles (18). Interestingly, a possible *N*-glycosylation site, Asn-562-Thr-Thr, is mapped in this region. *N*-glycosylation is an unusual posttranslational modification for nonenveloped viruses, except for rotaviruses (43). The mutant capsid mt12, which has substitutions of Asn-562 and Thr-564 to alanine, exhibited the same migration as the wild-type protein in SDS/PAGE, suggesting that the HEV-LP produced in insect cells was not glycosylated at Asn-562. Lack of *N*-glycosylation in the capsid protein has also been reported in mammalian cells infected with HEV (18), whereas some portion of the capsid protein was glycosylated and transported to the cell surface upon overexpression in mammalian cells (19). *N*-glycosylation of the HEV capsid at Asn-562 may have a negative effect on the receptor-binding, whereas it may play a positive role in other functions, including pathogenesis. The biological significance of the glycosylation of HEV capsid protein remains to be studied.

Although there is currently a lack of sensitive and reliable assays to determine the neutralizing activity of anti-HEV antibodies, the assay of NOB of HEV-LP binding to the target cells is thought to be a suitable alternative method. Measurement of the reactivity of a panel of mutant HEV-LPs revealed that the epitopes of MAB1323 and MAB272 antibodies are mapped in the peripheral region of the apical surface and the horizontal region of the P domain dimer, respectively. These results further support the notion that the P domain of HEV-LP is important for the binding to cells. MAB1323 is suggested to directly inhibit the interaction between HEV-LP and cellular receptors through binding to the apical surface, whereas MAB272 may have an allosteric effect, inducing conformational change of the P domain through binding to the horizontal region. A number of monoclonal antibodies are capable of neutralizing in vitro and in vivo infection of HEV (12–17), and many of them recognize conformational epitopes

of the capsid protein, as seen in the MAB1323 and MAB272 antibodies prepared in this study. Monoclonal antibodies against linear epitopes located in amino acids 578–607 of a genotype 1 capsid protein (16) were overlapped with a part of the putative receptor-binding domain and the epitope of MAB272, supporting the data of the present study. On the other hand, monoclonal antibodies against the linear epitopes located in amino acids 423–438 and amino acids 423–443 in the M domain of a genotype 1 capsid protein neutralized binding of a peptide derived from the capsid protein to cells and HEV-infection (13), suggesting the importance of the M domain in the binding step.

In summary, we have determined the crystal structure of HEV-LP produced in insect cells and demonstrated its structural characteristics in comparison with the structurally related animal and plant viruses. This study will provide useful information for elucidation of the molecular mechanisms of HEV-life cycles and for the development of prophylactic and therapeutic measures for hepatitis E.

Materials and Methods

Expression, Purification, and Crystallization of HEV-LP. The recombinant baculovirus encoding the ORF2 of the HEV genotype 3, 2712 strain was expressed in insect cells. HEV-LP was purified as described previously (28) and crystallized by the hanging-drop vapor-diffusion method. Details are reported in *SI Materials and Methods*.

Data Collection and Phase Determination. x-ray diffraction data were collected at 100 K on beamlines BL17A at the Photon Factory (KEK). The statistics of X-ray diffraction data collection are summarized in Table 1. The solved 3D structure of HEV-LP was submitted to the Protein Data Bank under the PDB accession code of 2ZTN. Details are reported in *SI Materials and Methods*.

ACKNOWLEDGMENTS. We thank H. Murase for her secretarial work and the staff of SPring-8 BL44XU beamline and synchrotron beamline NW-17A of the Photon Factory, High Energy Accelerator Research Organization for their assistance with the data collection. This work was supported in part by grants-in-aid from the Research and Development Program for New Bio-industry Initiatives of Bio-oriented Technology Research Advancement Institution (BRAIN) and the Foundation for Research Collaboration Center on Emerging and Re-emerging Infections.

1. Panda SK, Thakral D, Rehman S (2007) Hepatitis E virus. *Rev Med Virol* 17:151–180.
2. Purcell RH, Emerson SU (2008) Hepatitis E: An emerging awareness of an old disease. *J Hepatol* 48:494–503.
3. Navaneethan U, Al Mohajer M, Shata MT (2008) Hepatitis E and pregnancy: Understanding the pathogenesis. *Liver Int* 28:1190–1199.
4. Meng XJ, *et al.* (1997) A novel virus in swine is closely related to the human hepatitis E virus. *Proc Natl Acad Sci USA* 94:9860–9865.
5. Sonoda H, *et al.* (2004) Prevalence of hepatitis E virus (HEV) infection in wild boars and deer and genetic identification of a genotype 3 HEV from a boar in Japan. *J Clin Microbiol* 42:5371–5374.
6. Okamoto H (2007) Genetic variability and evolution of hepatitis E virus. *Virus Res* 127:216–228.
7. Li TC, *et al.* (2005) Hepatitis E virus transmission from wild boar meat. *Emerg Infect Dis* 11:1958–1960.
8. Yazaki Y, *et al.* (2003) Sporadic acute or fulminant hepatitis E in Hokkaido, Japan, may be food-borne, as suggested by the presence of hepatitis E virus in pig liver as food. *J Gen Virol* 84:2351–2357.
9. Tam AW, *et al.* (1991) Hepatitis E virus (HEV): Molecular cloning and sequencing of the full-length viral genome. *Virology* 185:120–131.
10. Matsubayashi K, *et al.* (2004) Transfusion-transmitted hepatitis E caused by apparently indigenous hepatitis E virus strain in Hokkaido, Japan. *Transfusion* 44:934–940.
11. Huang FF, *et al.* (2004) Determination and analysis of the complete genomic sequence of avian hepatitis E virus (avian HEV) and attempts to infect rhesus monkeys with avian HEV. *J Gen Virol* 85:1609–1618.
12. Emerson SU, *et al.* (2006) Putative neutralization epitopes and broad cross-genotype neutralization of Hepatitis E virus confirmed by a quantitative cell-culture assay. *J Gen Virol* 87:697–704.
13. He S, *et al.* (2008) Putative receptor-binding sites of hepatitis E virus. *J Gen Virol* 89:245–249.
14. Meng J, *et al.* (2001) Identification and characterization of the neutralization epitope(s) of the hepatitis E virus. *Virology* 288:203–211.
15. Takahashi M, *et al.* (2008) Production of monoclonal antibodies against hepatitis E virus capsid protein and evaluation of their neutralizing activity in a cell culture system. *Arch Virol* 153:657–666.
16. Schofield DJ, Glamann J, Emerson SU, Purcell RH (2000) Identification by phage display and characterization of two neutralizing chimpanzee monoclonal antibodies to the hepatitis E virus capsid protein. *J Virol* 74:5548–5555.
17. Schofield DJ, Purcell RH, Nguyen HT, Emerson SU (2003) Monoclonal antibodies that neutralize HEV recognize an antigenic site at the carboxyterminus of an ORF2 protein vaccine. *Vaccine* 22:257–267.
18. Graff J, *et al.* (2008) Mutations within potential glycosylation sites in the capsid protein of hepatitis E virus prevent the formation of infectious virus particles. *J Virol* 82:1185–1194.
19. Zafrullah M, Ozdener MH, Kumar R, Panda SK, Jameel S (1999) Mutational analysis of glycosylation, membrane translocation, and cell surface expression of the hepatitis E virus ORF2 protein. *J Virol* 73:4074–4082.
20. Huang R, *et al.* (1999) Cell culture of sporadic hepatitis E virus in China. *Clin Diagn Lab Immunol* 6:729–733.
21. Kazachkov Yu A, *et al.* (1992) Hepatitis E virus in cultivated cells. *Arch Virol* 127:399–402.
22. Meng J, Dubreuil P, Pillot J (1997) A new PCR-based seroneutralization assay in cell culture for diagnosis of hepatitis E. *J Clin Microbiol* 35:1373–1377.
23. Tam AW, *et al.* (1997) In vitro infection and replication of hepatitis E virus in primary cynomolgus macaque hepatocytes. *Virology* 238:94–102.
24. Tanaka T, Takahashi M, Kusano E, Okamoto H (2007) Development and evaluation of an efficient cell-culture system for Hepatitis E virus. *J Gen Virol* 88:903–911.
25. Bradley D, *et al.* (1988) Aetiological agent of enterically transmitted non-A, non-B hepatitis. *J Gen Virol* 69:731–738.
26. Li TC, *et al.* (1997) Expression and self-assembly of empty virus-like particles of hepatitis E virus. *J Virol* 71:7207–7213.
27. Li TC, *et al.* (2005) Essential elements of the capsid protein for self-assembly into empty virus-like particles of hepatitis E virus. *J Virol* 79:12999–13006.
28. Xing L, *et al.* (1999) Recombinant hepatitis E capsid protein self-assembles into a dual-domain T = 1 particle presenting native virus epitopes. *Virology* 265:35–45.
29. Prasad BV, *et al.* (1999) X-ray crystallographic structure of the Norwalk virus capsid. *Science* 286:287–290.
30. Chen R, Neill JD, Estes MK, Prasad BV (2006) X-ray structure of a native calicivirus: Structural insights into antigenic diversity and host specificity. *Proc Natl Acad Sci USA* 103:8048–8053.
31. Morgunova E, *et al.* (1994) The atomic structure of Carnation Mottle Virus capsid protein. *FEBS Lett* 338:267–271.
32. Hogle JM, Chow M, Filman DJ (1985) Three-dimensional structure of poliovirus at 2.9 A resolution. *Science* 229:1358–1365.
33. Tsao J, *et al.* (1991) The three-dimensional structure of canine parvovirus and its functional implications. *Science* 251:1456–1464.
34. Bhella D, Gatherer D, Chaudhry Y, Pink R, Goodfellow IG (2008) Structural insights into calicivirus attachment and uncoating. *J Virol* 82:8051–8058.
35. Bu W, *et al.* (2008) Structural basis for the receptor binding specificity of Norwalk virus. *J Virol* 82:5340–5347.
36. Choi JM, Hutson AM, Estes MK, Prasad BV (2008) Atomic resolution structural characterization of recognition of histo-blood group antigens by Norwalk virus. *Proc Natl Acad Sci USA* 105:9175–9180.
37. Li TC, *et al.* (2004) Protection of cynomolgus monkeys against HEV infection by oral administration of recombinant hepatitis E virus-like particles. *Vaccine* 22:370–377.
38. Hsu C, *et al.* (2006) Characterization of polymorphism displayed by the coat protein mutants of tomato bushy stunt virus. *Virology* 349:222–229.
39. Kakani K, Reade R, Katpally U, Smith T, Rochon D (2008) Induction of particle polymorphism by cucumber necrosis virus coat protein mutants in vivo. *J Virol* 82:1547–1557.
40. White LJ, Hardy ME, Estes MK (1997) Biochemical characterization of a smaller form of recombinant Norwalk virus capsids assembled in insect cells. *J Virol* 71:8066–8072.
41. Belnap DM, *et al.* (2000) Molecular tectonic model of virus structural transitions: The putative cell entry states of poliovirus. *J Virol* 74:1342–1354.
42. Bubeck D, Filman DJ, Hogle JM (2005) Cryo-electron microscopy reconstruction of a poliovirus-receptor-membrane complex. *Nat Struct Mol Biol* 12:615–618.
43. Jayaram H, Estes MK, Prasad BV (2004) Emerging themes in rotavirus cell entry, genome organization, transcription and replication. *Virus Res* 101:67–81.

Acta Crystallographica Section F
Structural Biology and Crystallization Communications
ISSN 1744-3091

Crystallization and preliminary X-ray diffraction analysis of recombinant hepatitis E virus-like particle

Che-Yen Wang,[a,b,c]‡ Naoyuki Miyazaki,[a,b,d]‡ Tetsuo Yamashita,[d,e]‡ Akifumi Higashiura,[d] Atsushi Nakagawa,[d] Tian-Cheng Li,[f] Naokazu Takeda,[f] Li Xing,[a,b] Erik Hjalmarsson,[g] Claes Friberg,[g] Der-Ming Liou,[c] Yen-Jen Sung,[c,h] Tomitake Tsukihara,[d] Yoshiharu Matsuura,[e] Tatsuo Miyamura[f] and R. Holland Cheng[a,b]*

[a]Molecular and Cellular Biology, University of California, Davis, CA 95616, USA, [b]Karolinska Institute Structural Virology, F68 Karolinska University Hospital, SE-14186 Stockholm, Sweden, [c]Institute of Public Health, National Yang-Ming University, 112 Taipei, Taiwan, [d]Institute for Protein Research, Osaka University, 3-2 Yamadaoka, Suita, Osaka 565-0871, Japan, [e]Institute for Microbial Diseases, Osaka University, 3-2 Yamadaoka, Suita, Osaka 565-0871, Japan, [f]Department of Virology II, National Institute of Infectious Diseases, Tokyo, Japan, [g]Crystal Research AB, 22370 Lund, Sweden, and [h]Institute of Anatomy and Cell Biology, National Yang-Ming University, 112 Taipei, Taiwan

‡ These authors contributed equally to the work.

Correspondence e-mail: rhch@ucdavis.edu

Received 3 March 2008
Accepted 16 March 2008

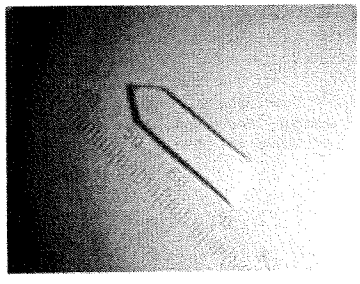

Hepatitis E virus (HEV) accounts for the majority of enterically transmitted hepatitis infections worldwide. Currently, there is no specific treatment for or vaccine against HEV. The major structural protein is derived from open reading frame (ORF) 2 of the viral genome. A potential oral vaccine is provided by the virus-like particles formed by a protein construct of partial ORF3 protein (residue 70–123) fused to the N-terminus of the ORF2 protein (residues 112–608). Single crystals obtained by the hanging-drop vapour-diffusion method at 293 K diffract X-rays to 8.3 Å resolution. The crystals belong to space group $P2_12_12_1$, with unit-cell parameters $a = 337$, $b = 343$, $c = 346$ Å, $\alpha = \beta = \gamma = 90°$, and contain one particle per asymmetric unit.

1. Introduction

The hepatitis E virus (HEV) is a naked icosahedral capsid with a single-stranded positive-sense RNA of 7.2 kbp. The genome encodes three open reading frames (ORFs). ORF1, mapped to the 5′-terminus, encodes nonstructural proteins that are mainly involved in virus replication and protein processing. ORF2, mapped to the 3′-terminus, encodes a viral capsid protein of 660 amino acids that has been found to elicit neutralizing antibodies (Meng *et al.*, 2001; Schofield *et al.*, 2000). ORF3, mapped between ORF1 and ORF2, encodes a protein of 123 amino-acid residues that may interfere with control functions within the infected cell, as summarized by Panda *et al.* (2007). When the N-terminally truncated ORF2 protein (residues 112–660) was expressed with a recombinant baculovirus in an insect-cell line, self-assembling virus-like particles (VLPs) were released into the cell supernatant (Li *et al.*, 1997). These VLPs have been shown to induce anti-HEV antibodies when orally administered to experimental animals (Li *et al.*, 2004). By N- and C-terminal sequencing, the VLP-forming protein was found to be composed of residues 112–608 of the ORF2 protein (VLP_{ORF2}); thus, 52 residues at the C-terminus were cleaved during VLP formation (Li *et al.*, 1997). We have previously reported the structure of HEV-VLP_{ORF2} obtained using electron cryomicroscopy (cryo-EM), which provided a preliminary understanding of the quaternary arrangement of the viral capsids. A three-dimensional reconstruction of VLP_{ORF2} displays $T = 1$ icosahedral symmetry and is composed of 60 copies of the truncated ORF2 protein (Xing *et al.*, 1999; Li *et al.*, 2005).

Although a truncated ORF2 polypeptide is undergoing clinical trials as a vaccine candidate (Shrestha *et al.*, 2007), to date no specific treatment or vaccine has been licensed for HEV (Purcell & Emerson, 2008). The viral capsid is an important form of presenting the conformation-dependent epitopes (Maloney *et al.*, 2005) and HEV-VLP_{ORF2} has been proposed as a suitable candidate for an oral vaccine (Li *et al.*, 2004). Further investigations of the high-resolution structural features of a VLP are required in order to establish the folding and interactions of the viral protein in the context of the HEV particle form, as well as to characterize the immunogenic epitopes that are responsible for inducing the neutralizing antibodies. In the present study, we describe the crystallization and preliminary crys-